AD-A099 225   MCDONNELL DOUGLAS RESEARCH LABS ST LOUIS MO   F/G 11/9
MAGNETIC RESONANCE STUDIES OF EPOXY RESINS.(U)
DEC 80   I M BROWN, A C LIND, T C SANDRECZKI   N00019-79-C-0414
UNCLASSIFIED   MDC-Q0721   NL

1 OF 1
AD A
099225

END
DATE
FILMED
6-81
DTIC

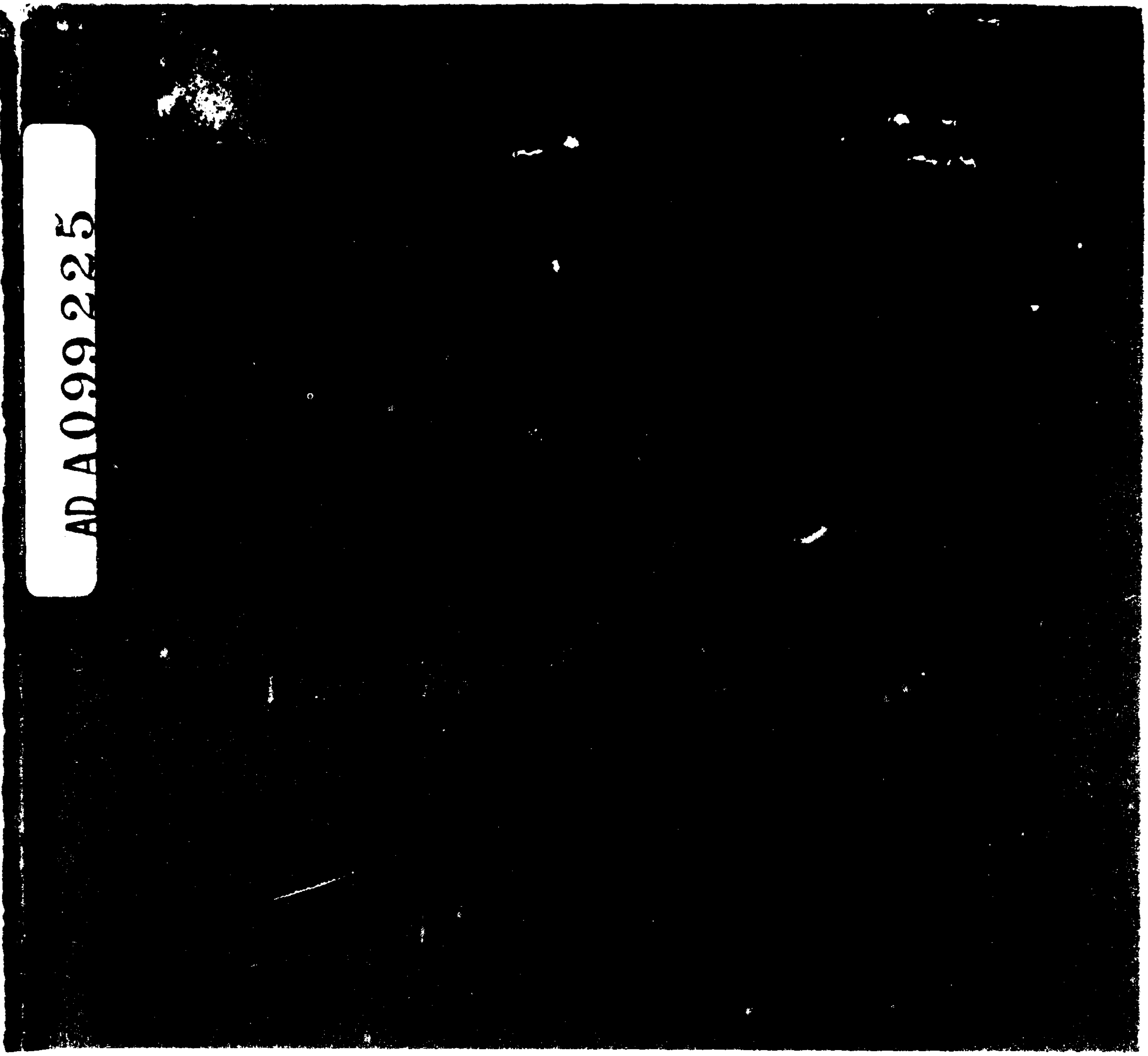

MCDONNELL DOUGLAS RESEARCH LABORATORIES

MCDONNELL DOUGLAS
CORPORATION

UNCLASSIFIED

SECURITY CLASSIFICATION OF THIS PAGE (When Data Entered)

REPORT DOCUMENTATION PAGE

READ INSTRUCTIONS BEFORE COMPLETING FORM

14

1. REPORT NUMBER: MDC-Q0721	2. GOVT ACCESSION NO.: AD-A099225
3. RECIPIENT'S CATALOG NUMBER	
4. TITLE (and Subtitle): MAGNETIC RESONANCE STUDIES OF EPOXY RESINS	5. TYPE OF REPORT & PERIOD COVERED: Final Report 7 Sep 79 — 7 Dec 80
	6. PERFORMING ORG. REPORT NUMBER
7. AUTHOR(s): I. M. Brown, A. C. Lind, T. C. Sandreczki	8. CONTRACT OR GRANT NUMBER(s): N00019-79-C-0414
9. PERFORMING ORGANIZATION NAME AND ADDRESS: McDonnell Douglas Research Laboratories, McDonnell Douglas Corporation, St. Louis, Missouri 63166	10. PROGRAM ELEMENT, PROJECT, TASK AREA & WORK UNIT NUMBERS
11. CONTROLLING OFFICE NAME AND ADDRESS: Department of the Navy, Naval Air Systems Command, Washington, DC 20361	12. REPORT DATE: 7 December 1980
	13. NUMBER OF PAGES: 80
14. MONITORING AGENCY NAME & ADDRESS (if different from Controlling Office): 12 83	15. SECURITY CLASS. (of this report): Unclassified
	15a. DECLASSIFICATION/DOWNGRADING SCHEDULE

16. DISTRIBUTION STATEMENT (of this Report)

Approved for public release; distribution unlimited.

DTIC ELECTE MAY 21 1981 G

17. DISTRIBUTION STATEMENT (of the abstract entered in Block 20, if different from Report)

18. SUPPLEMENTARY NOTES

19. KEY WORDS (Continue on reverse side if necessary and identify by block number)

Epoxy resins	Electron paramagnetic resonance	Water plasticizer
Spin probes	Nuclear magnetic resonance	Quaternary salts
Spin labels	Local mode of segmental motion	Relaxation times
Hydrolysis	Glass transition temperature	

20. ABSTRACT (Continue on reverse side if necessary and identify by block number)

Electron paramagnetic resonance (EPR) and hydrogen nuclear magnetic resonance (NMR) were used to investigate main-chain molecular motions in the epoxy resins tetraglycidyldiaminodiphenylmethane (TGDDM) and diglycidyl ether of bisphenol A (DGEBA) cured with dimethyldiaminohexane (DDH) and diethylenetriamine (DETA). The cured resins were studied close to the glass transition as a function of temperature and as a function of solvent content (methylene chloride and water).

DD FORM 1 JAN 73 1473 EDITION OF 1 NOV 65 IS OBSOLETE

UNCLASSIFIED

SECURITY CLASSIFICATION OF THIS PAGE (When Data Entered)

405315

In the EPR approach, stable nitroxide free radicals were used either as spin probes or spin labels to probe their dynamic environment in the polymer. The uncured TGDDM was spin labeled at the epoxy group with nitroxide amines to form either an end label or a quaternary base. The latter was found to undergo a Hofmann elimination reaction to release a stable nitroxide spin probe.

In the dry cured epoxy resins at each temperature, the EPR lineshapes of the spin labels and spin probes could be characterized by one value of the motional correlation time. The temperature dependence of this motional correlation time obeys the WLF equation. On the other hand, at some solvent contents, the EPR lineshapes could be resolved into two spectra associated with a slow phase and a fast phase indicating a bimodal distribution of motional correlation times. The solvent dependence of the motional correlation times for the fast phases obeyed a modified form of the Fujita-Doolittle equation. The two phases were identified with nitroxides located in regions with different microstructures, viz., regions with high crosslink density (the slow phase) embedded in and bound to regions of low crosslink density (the fast phase). The motion of the spin labels in the fast phase was attributed to a local mode located on the main chain, whereas the motion of the spin probes in the fast phase was the result of either main-chain segmental motions or local modes that precede the onset of the segmental motions.

In the NMR experiments, pulsed techniques were used to measure the relative number of hydrogens in mobile and rigid regions of dry and wet cured epoxy resins of varying composition. The relaxation times of the hydrogens in both regions were measured and used to determine the molecular motions, and spectral data were obtained to identify those molecular groups undergoing extensive motion. Multi-pulse techniques were employed to determine the sizes of the mobile and rigid regions in samples containing sorbed water.

PREFACE

This report is an account of the work performed by the McDonnell Douglas Research Laboratories on the Magnetic Resonance Studies of Epoxy Resins for the Naval Air Systems Command, Contract No. N00019-79-C-0414, from 7 September 1979 to 7 December 1980. The work was performed in the Chemical Physics Department, managed by Dr. D. P. Ames. The principal investigators were Dr. I. M. Brown and Dr. A. C. Lind; Dr. T. C. Sandreczki was a co-investigator. The project monitor was Mr. R. Dempsey, Naval Air Systems Command, Washington, DC.

TABLE OF CONTENTS

LIST OF ILLUSTRATIONS

LIST OF ILLUSTRATIONS

LIST OF ILLUSTRATONS

Figure Page

LIST OF ILLUSTRATIONS

LIST OF TABLES

1. INTRODUCTION

Epoxy resin polymers are important matrix materials for composite structural components in military aircraft. At present there is considerable evidence that the polymeric network in cured epoxy resins contains regions of nonuniform crosslink density.[1-7] These network inhomogeneities consist of regions of high crosslink density, variously referred to as globules,[2] nodules[3] or domains,[7] embedded in and bound to regions of low crosslink density. It is important to characterize these network inhomogeneities because of the consequences of network morphology on the long-term behavior of the mechanical properties such as yield strength and toughness.[5]

In this study we used the magnetic resonance techniques, electron paramagnetic resonance (EPR) and nuclear magnetic resonance (NMR), to obtain information on this network microstructure. The experiments involved measurements made as a function of either temperature or solvent content. In the latter case, the experiments also included the study of the effect of sorbed water on the network microstructure, which is of particular relevance since the sorbed water is known to decrease the high-temperature mechanical properties as well as lower the glass transition temperature.[8]

Since epoxy resins are diamagnetic, nitroxide free radicals were used in the EPR experiments as probes of their dynamic environments in the polymer. The nitroxide was employed either as a spin label where it was covalently bound at a known site in the polymer or as a spin probe where it was randomly distributed throughout the polymer. Since in both cases the nitroxide was sensitive to the local free volume in the polymer, it could be used to probe the main-chain motions associated with the glass transition in the different regions of the network microstructure. The EPR lineshapes are sensitive to the motion of the nitroxide molecule over a range of motional correlation time, τ_c, given by $\tau_c = 10^{-7}$ to 10^{-11} s.[9] In the fast motion regime ($\tau_c = 10^{-11}$ to 5×10^{-9} s), the motional correlation time can be evaluated using the theory of Kivelson[10], whereas in the slow motion regime ($\tau_c = 5 \times 10^{-9}$ to 10^{-7} s), the values can be obtained by computer simulation or using an analytical technique.[11]

Pulsed hydrogen NMR techniques were used to measure spin-spin and spin-lattice relaxation times and chemical-shift spectra of solid epoxies. The relaxation time data reveal molecular motion with a correlation time τ_c between 10^{-4} and 10^{-9} s,[12] and the chemical shift spectra identify the molecular groups undergoing extensive motion. The spin-spin relaxation time increases abruptly at the onset of extensive molecular motion associated with the glass transition, and the value to which it increases provides a qualitative measure of the average crosslink density. The relative amounts of mobile and rigid phases and the sizes of the mobile and rigid regions can be determined using multiple-pulse techniques.[13-15]

2. EPR EXPERIMENTS ON EPOXY RESINS

2.1 EPR Sample Preparation

The epoxy resins studied were the diglycidyl ether of bisphenol A (DGEBA) and tetraglycidyldiaminodiphenylmethane (TGDDM). The commercial resins used were DER 332 (DGEBA) obtained from the Dow Chemical Company and MY720 (the main constituent is TGDDM) obtained from the Ciba Geigy Company. These resins were cured with dimethyldiaminohexane (DDH) obtained from Eastman Kodak Company and diethylene triamine (DETA) obtained from Aldrich Chemical Company. The molecular structures of these compounds are shown in Figure 1. Both of these curing agents were used without further purification.

The epoxy resins were spin labeled with the nitroxide amines, 4-amino-2,2,6,6-tetramethylpiperidine-1-oxyl (TAMIN), 4-methylamino-2,2,6,6-tetramethylpiperidine-1-oxyl (METAMIN), 4-dimethylamino-2,2,6,6-tetramethylpiperidine-1-oxyl (DIMETAMIN), and 3-(N-methyl-N-(6-methylaminohexyl)carbamoyl-2,2,5,5-tetramethylpyrroline-1-oxyl (PYRODDH). Complementary experiments involving the spin probes 4-hydroxy-2,2,6,6-tetramethylpiperidine-1-oxyl (TANOL), and 2,2,6,6-tetramethyl-1,2,3,6-tetrahydropyridine-1-oxyl (TEMPENE) in cured epoxy samples were also performed. The structures of these nitroxides are shown in Figure 2.

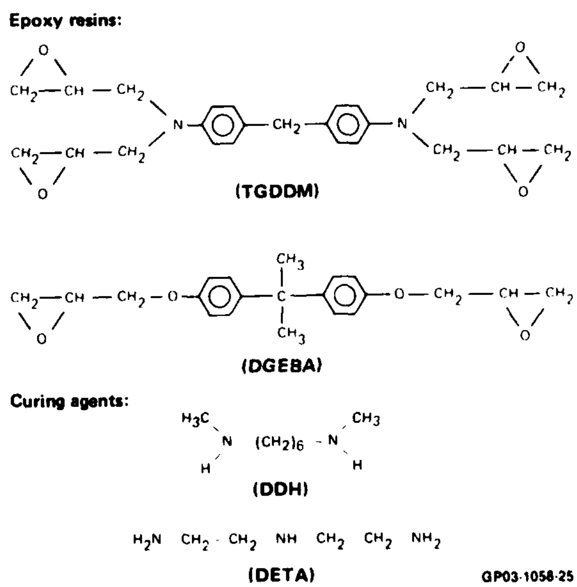

Figure 1. Epoxy resins and curing agents used.

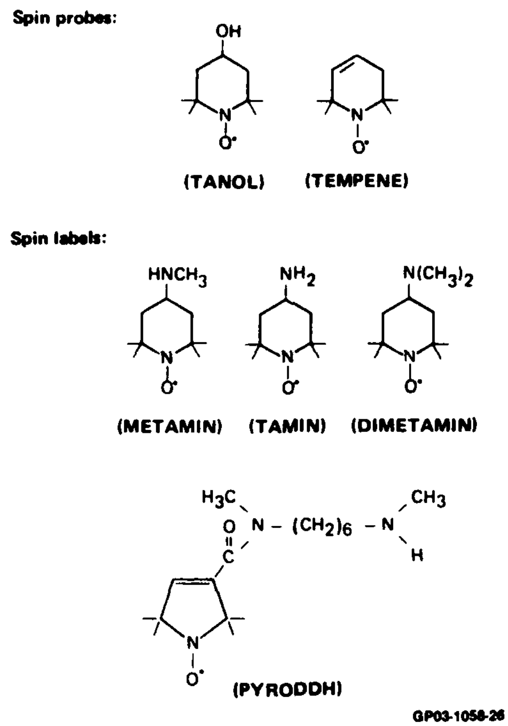

Figure 2. Spin probes and spin labels used.

A previous study[12] indicated that an epoxy labeled with METAMIN or TAMIN was too rigid in the cured epoxy. A more mobile spin label attached to the oxirane ring by way of a flexible aliphatic chain was therefore sought, and PYRODDH was chosen for study because of the relative ease of the following synthesis.

The imidazole derivative of 3-carboxy-2,2,5,5-tetramethylpyrroline-1-oxyl (CPNO) was first prepared as an intermediate product. This imidazole intermediate (IPNO) was prepared from CPNO and carbonyldiimidazole (CD) as follows: while stirring, 13.6 milliequivalents of CPNO were added to a solution of 26.1 milliequivalents of CD in 100 mL of chloroform. After additional stirring in a dry nitrogen atmosphere for 1 h, the mixture was extracted three times with water, dried with molecular sieves, and filtered to remove suspended matter. The solvent was then evaporated with a stream of nitrogen, and the solid residue was recrystallized twice from methylcyclohexane to yield long yellow needles which were collected by filtration and dried under vacuum.

PYRODDH was prepared from the IPNO intermediate (see Figure 3) by adding a solution of 3 milliequivalents of IPNO in chloroform to 6 milliequivalents of DDH followed by stirring overnight to yield a product that contained approximately 50% PYRODDH, 25% PYRODDH biradical, and 25% unreacted DDH. The PYRODDH and DDH were removed from the mixture by extraction with a dilute aqueous HCl solution, followed by addition of a NaOH solution to the aqueous layer, and extraction of this aqueous solution with chloroform. The EPR spectrum of the resulting chloroform solution revealed that no biradical was present.

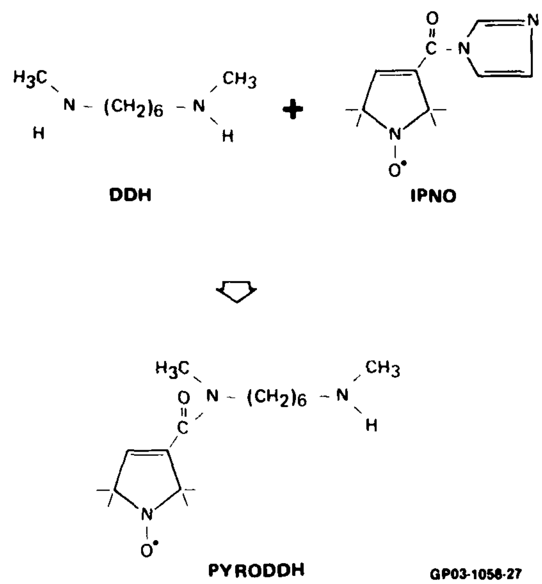

Figure 3. Synthesis of PYRODDH from DDH and IPNO.

Attempts at further purification of the PYRODDH using normal-phase and reverse-phase thin-layer chromatography, recrystallization and high-pressure liquid chromatography (HPLC) with C_{18}, phenyl, and nitrile functionality columns proved unsuccessful. More encouraging results were obtained using gel permeation chromatography (GPC) and using HPLC with a column having amine functionality. However, the times required for complete isolation of the product by these methods proved prohibitive. It was therefore decided that since the partially purified PYRODDH had no biradical contamination, it was satisfactory for use as a spin label.

In the typical preparation of a cured sample of DGEBA containing a spin probe, the following procedure was followed. Approximately 0.1 wt% nitroxide was dissolved in DGEBA, which previously had been heated (~ 335 K) to melt any crystals present. The appropriate amount of curing agent was added, and the mixture was thoroughly stirred, heated (~ 320 K), and degassed in a vacuum oven until all air bubbling ceased. The mixture was then poured into either flexible silicone rubber molds (G.E. type RTV 664 silicone compound was found convenient) or clean 5 mL glass vials where it was allowed to cure at 293 K for at least 20 h.

Cured MY720 samples containing spin probes had to be prepared in a slightly different manner because of the higher viscosity of the MY720 resin at 293 K. The sample preparation involved either dissolving 0.1 wt% nitroxide into the resin at 335 K followed by cooling to 293 K and adding the curing agent or mixing the curing agent, nitroxide, and resin simultaneously at 293 K whereby the viscosity of the mixture was lowered. Degassing of the mixtures and pouring into molds followed by curing for 20 h completed the sample preparation.

2.2 Spin Labeling Reactions in the Uncured MY720 Epoxy Resin

First the EPR results of the spin labeling experiments obtained when METAMIN reacted with the MY720 resin at 363 K are discussed. The spectra were recorded at four temperatures: 296 K, 336 K, 345 K, and 356 K, after the reaction was allowed to proceed at 363 K for different times. In the course of the reaction, a sequence of different spin labels and spin probes could be distinguished by their EPR spectra. Immediately after mixing METAMIN with MY720, the spectrum of the unreacted spin probe METAMIN was observed (the peaks in this spectrum are designated P in Figure 4). As the reaction proceeded at 363 K, the spectrum of a more rigid species developed (the peaks in this spectrum are denoted by E in Figure 4) and increased in intensity as the intensity of the P peaks decreased. This process is illustrated in Figures 4 and 5 which show the spectra recorded at 296 K, 336 K, 345 K, and 356 K, 36 min and 15 h after the initiation of the reaction, respectively. As shown in Figures 4 and 5, only above 300 K is it possible to detect more than one spectrum. On further heating of the MY720 samples, a third spectrum associated with an even more rigid species appeared. This spectrum (the peaks

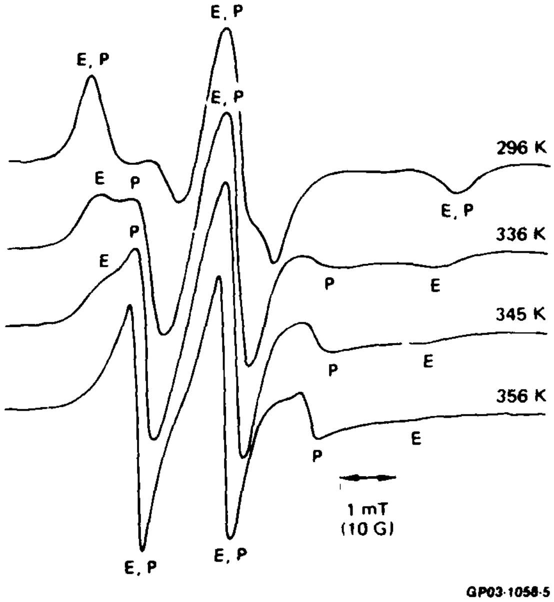

Figure 4. The EPR spectra observed at 296 K, 336 K, 345 K, and 356 K from a sample of MY720 containing METAMIN after 36 min heating at 363 K. The derivative peaks associated with the probe and end label are designated P and E, respectively.

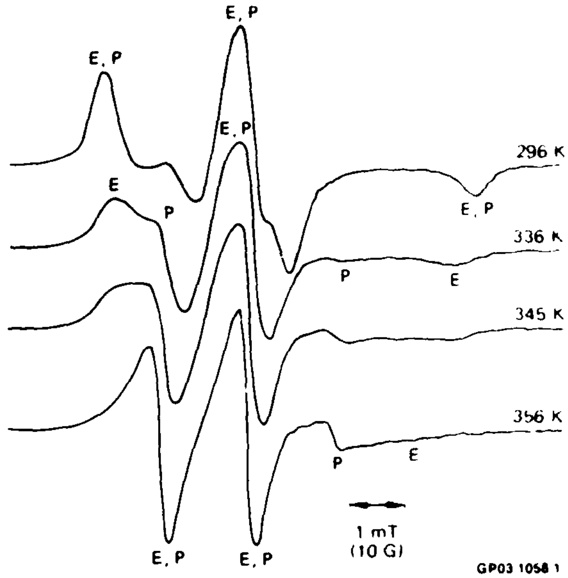

Figure 5. The EPR spectra observed at 296 K, 336 K, 345 K, and 356 K from a sample of MY720 containing METAMIN after 15 h heating at 363 K. The derivative peaks associated with the probe and end label are designated P and E, respectively.

are designated Q in Figure 6) was accompanied by yet a fourth spectrum consisting of three narrow lines (marked T in Figure 6). In Figure 6, the spectrum T can be distinguished from the spectrum Q only above 300 K, although at 296 K there is an indication of an additional unresolved T peak in the center line.

As the reaction proceeded, the peak heights decreased because of a decrease of the total magnetic susceptibility. The total integrated absorption intensity decreased with time because the nitroxides were decomposing in the MY720 resin. After 8 h into the reaction at 363 K, this decrease was so great (over an order of magnitude) that achieving an adequate signal-to-noise ratio became a problem. It was therefore necessary to signal average the spectra using the data acquisition system (Varian E-900) for samples that had been heated for longer than 4 h. Most of the spectra shown in Figures 4 and 5 were the result of 25 scans, so that an improvement in signal-to-noise ratio of $\sqrt{25} = 5$ was realized.

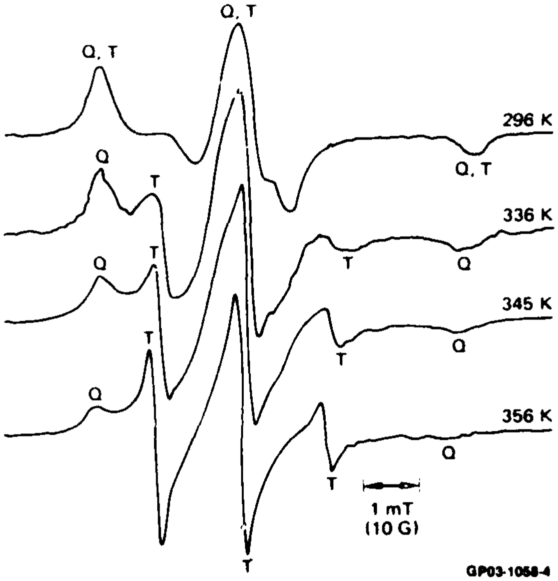

Figure 6. The EPR spectra observed at 296 K, 336 K, 345 K, and 356 K from a sample of MY720 containing METAMIN after 100 h heating at 363 K. The derivative peaks associated with the quaternary base and TEMPENE are designated Q and T, respectively.

In view of the results and conclusions in our previous study[16] with the DGEBA resin, the spectrum P is assigned to the spin probe METAMIN, the spectrum E to the TGDDM end-labeled with METAMIN (Figure 7), the spectrum Q to the spin-labeled quaternary base (Figure 7), and spectrum T to the spin probe TEMPENE (Figure 2). The latter forms as the result of a Hofmann elimination reaction[17] involving a molecular rearrangement and a scission of a carbon-nitrogen bond in the quaternary base. The formation of TEMPENE was conclusive evidence that its precursor, the spin-labeled quaternary base, formed and is the species that can be assigned to spectrum Q.

The onset of the motional narrowing, as indicated by the spectral collapse to three narrow lines, occurs at increasingly higher temperatures for the TEMPENE spin probe, the METAMIN spin probe, the end-labeled monomer, and the spin-labeled quaternary base, respectively. This feature indicates the increasing order of the motional correlation times for these species. Moreover, the large difference in extrema splittings that results from the difference in correlation times allows the spectral discrimination between the probe and the end label, the end label and the quaternary base, and the quaternary base and TEMPENE.

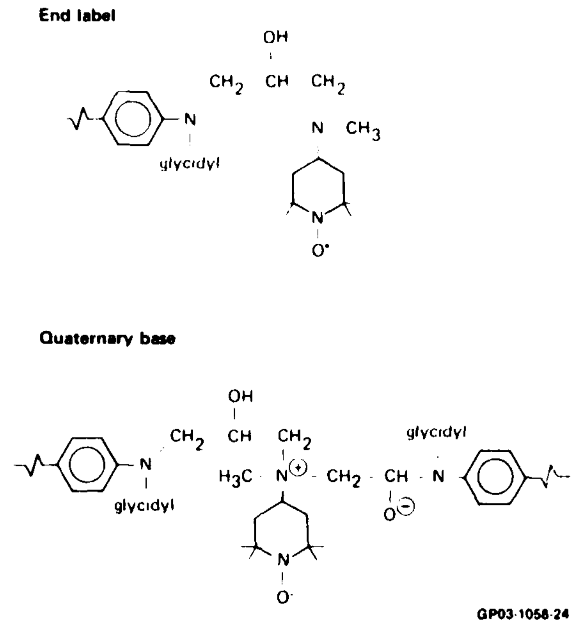

Figure 7. Structures for the end label and quaternary base formed when TGDDM is spin-labeled with METAMIN.

The motional correlation times can be determined by the size of the species in which case the pertinent motion is end-over-end molecular tumbling. Alternatively, the correlation times can also be affected by steric factors at the amino nitrogen position; the relevant motion is then a rotation about the carbon-nitrogen bond.

Analogous spectra have been observed in the course of the reaction of TAMIN with MY720, but the spectral interpretations are complicated by the nitroxide acting as a bridging group between two TGDDM molecules. Only one spectrum could be associated with the quaternary base and the bridging group. This observation implies that the motional correlation times for these species are comparable at all temperatures from 77 K to 360 K, and/or the amount of quaternary base present is always small. Yet the presence of TEMPENE as a decomposition product of the quaternary base in the Hofmann elimination reaction[13] is conclusive proof that its precursor, the quaternary base, has formed.

The corresponding spectra observed in the reactions of DIMETAMIN with MY720 are shown in Figures 8 and 9. In these reactions, only three different spectra were observed: those associated with the DIMETAMIN spin probe, the

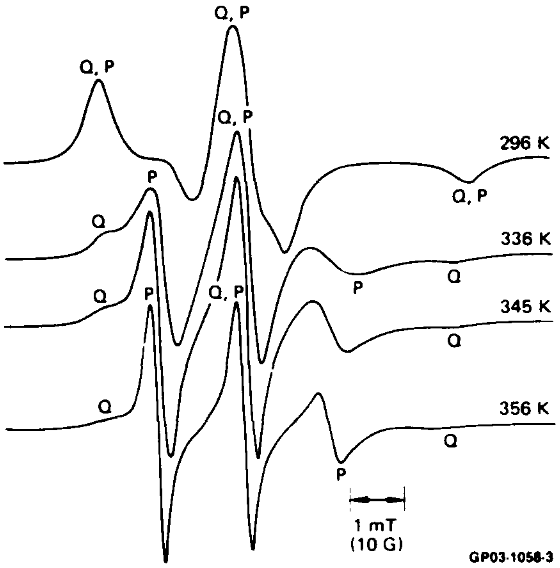

Figure 8. The EPR spectra observed at 296 K, 336 K, 345 K, and 356 K from a sample of MY720 containing DIMETAMIN after 15 min heating at 363 K. The derivative peaks associated with the probe and quaternary base are designated P and Q, respectively.

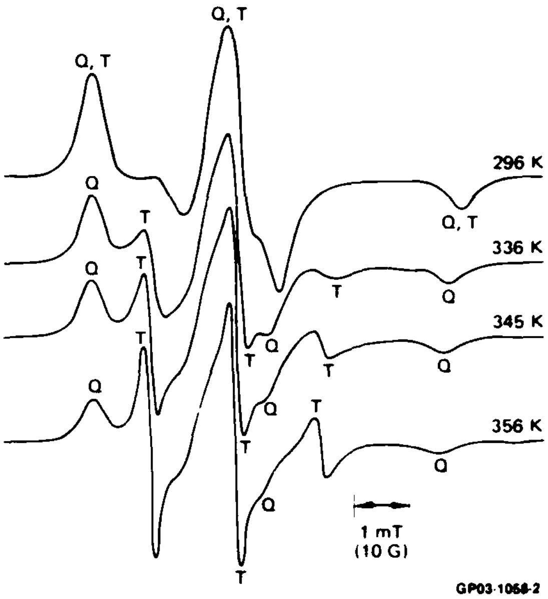

Figure 9. The EPR spectra observed at 296 K, 336 K, 345 K, and 356 K from a sample of MY720 containing DIMETAMIN after 90 min heating at 363 K. The derivative peaks associated with the quaternary base and TEMPENE are designated Q and T, respectively.

spin-labeled quaternary base (spectrum Q in Figures 8 and 9), and TEMPENE (spectrum T in Figure 9). These results are consistent with the above spectral assignments for the METAMIN and TAMIN reactions in MY720. Noting the time scale in Figures 8 and 9, the appearance of the quaternary base and TEMPENE (spectrum Q and spectrum T in Figures 8 and 9 respectively) occurred earlier in the reaction with DIMETAMIN than with METAMIN.

The total magnetic susceptibility also decreased with time because of the nitroxide decomposition in the MY720 resin. The resulting decrease of the EPR signals was, however, less critical because the reaction times for quaternary base formation with DIMETAMIN was shorter.

When PYRODDH was used to spin label uncured DGEBA, the formation of the end label and quaternary base (see Figure 10) were not clearly identifiable from the changes in the EPR lineshapes. Spectra of PYRODDH in DGEBA recorded at 313 K after different times into the reaction at 363 K are shown in Figure 11. Neither the spectrum of TEMPENE nor those associated with any Hofmann elimination products were observed. Thus, there was no positive proof that

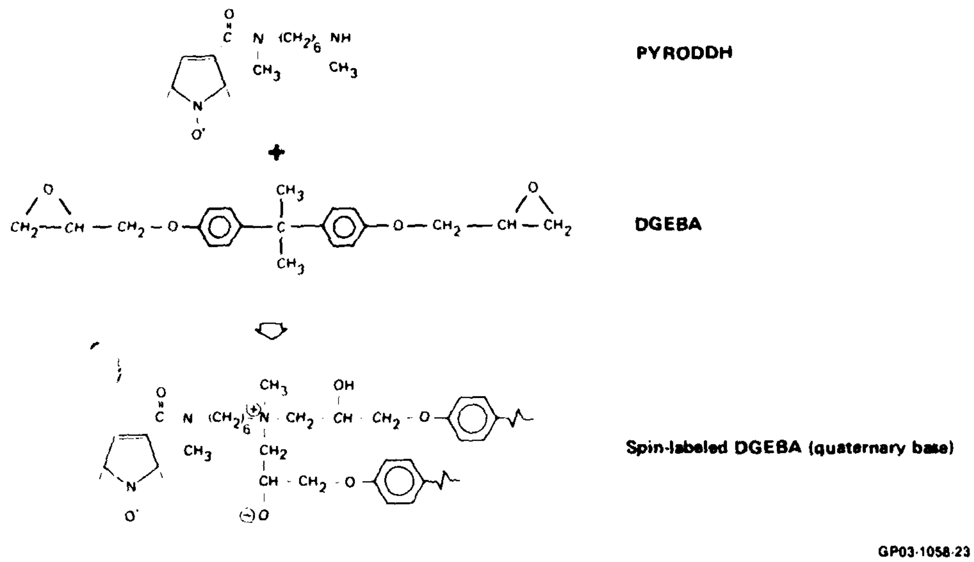

Figure 10. Quaternary base formation when DGEBA is labeled with PYRODDH.

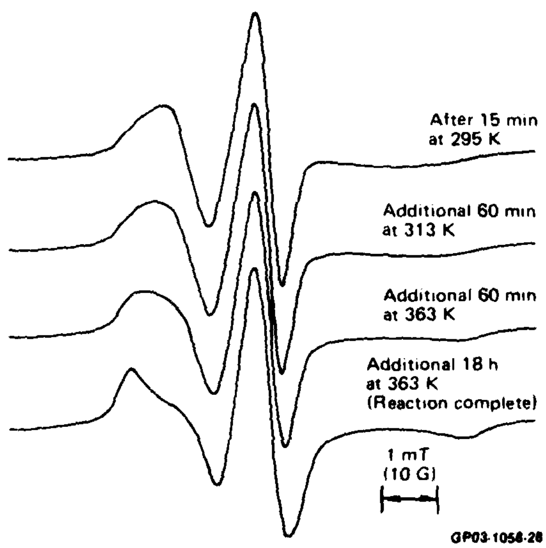

Figure 11. The EPR lineshapes observed as PYRODDH reacts with the uncured DGEBA resin to form the quaternary base spin label. All spectra were recorded at 313 K.

the PYRODDH was bound to two DGEBA molecules. However, the reaction appeared to be complete after ~ 18 h of heating at 363 K since heating for an additional 24 h produced no observable change in the lineshape. Considering the time scale for the quaternary base formation in DGEBA spin labeled with METAMIN, the spectral lineshape changes shown in Figure 11 would appear to provide evidence that the quaternary base was formed within 18 h in the reaction of PYRODDH with DGEBA at 363 K.

2.3 Spin Probes and Spin Labels in Cured Epoxy Samples

Samples of MY720 containing the spin probe TEMPENE were cured with a 1:1 stoichiometric amount of the curing agent DDH. Since the latter is primarily a bifunctional curing agent, the cured polymer formed is only lightly crosslinked. This low crosslinking is apparent since these samples can be extensively swelled with methylene chloride.

The temperature dependence of the EPR lineshapes of the spin probe TEMPENE in these cured samples was studied from 293 K to 420 K. Typical examples of the observed spectra are shown in Figure 12. With increasing temperature, the spectra exhibited the typical features indicating the onset of motional collapse and line narrowing. At all temperatures, the spectra can be characterized by essentially one motional correlation time or at most a narrow distribution of correlation times.

Motional correlation times in the range $\tau_c < 5 \times 10^{-9}$ s were evaluated from the EPR lineshapes using the theory of Kivelson.[10] The equation used was

$$\tau_c = 4\left[\left(\frac{Y(0)}{Y(1)}\right)^{1/2} + \left(\frac{Y(0)}{Y(-1)}\right)^{1/2} - 2\right] b^{-2}[T_2(0)]^{-1}, \qquad \text{(1a)}$$

with

$$b = \left(\frac{4\pi}{3}\right)\left[A_{zz} - \frac{1}{2}(A_{xx} + A_{yy})\right], \qquad \text{(1b)}$$

where Y(1), Y(0), and Y(-1) are the intensities of the low, middle, and high field lines, A_{xx}, A_{yy}, and A_{zz} are the principal values of the nitrogen hyperfine interaction tensor, and $[T_2(0)]^{-1}$ is the linewidth of the center line.

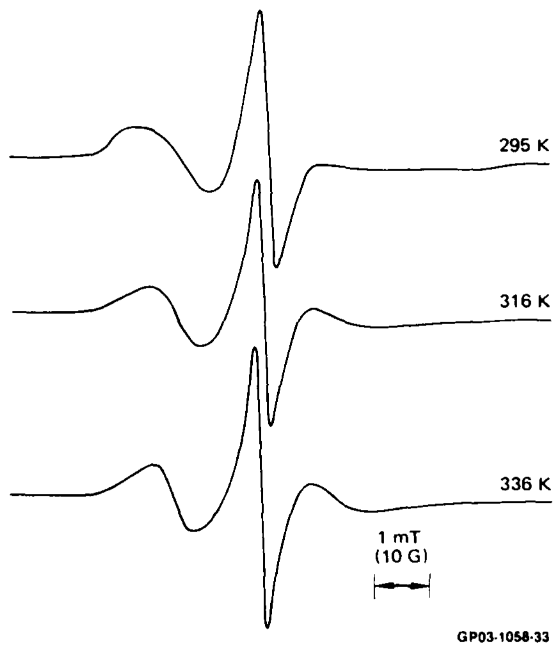

Figure 12. Temperature dependence of the EPR lineshapes for the spin probe TEMPENE in samples of MY720 cured with DDH (1:1 stoichiometry).

The WLF equation, which describes the temperature dependence of the relaxation behavior for a polymer above its T_g, can be written in the form[18]

$$\ln \alpha_T = \frac{B(T - T_R)}{f_R(f_R/\beta_R + T - T_R)} \tag{2a}$$

with the shift factor

$$\alpha_T = [\tau]_T/[\tau]_R , \tag{2b}$$

where $[\tau]_T$ and $[\tau]_R$ are the viscoelastic relaxation times at temperature T and a reference temperature T_R, respectively; f_R is the free-volume fraction at temperature T_R; β_R is the difference in thermal expansion coefficients above and below T_g; and B is the coefficient that appears in the Doolittle equation ($B \approx 1$).[19]

It seems reasonable to assume that the rotational diffusion coefficient for the spin probe (or spin label) has the same relationship to the free volume as does the monomeric translational diffusion coefficient for the polymer.[18] Hence, we assume

$$\alpha_T' = \frac{\tau_c}{\tau_{cR}} = \frac{[\xi_1]_T\, T_R}{[\xi_1]_R\, T} = \frac{D_{rR}}{D_{rT}}\,, \tag{3a}$$

whereas

$$\alpha_T = \frac{[\tau]_T}{[\tau]_R} = \frac{[\xi_o]_T\, T_R}{[\xi_o]_R\, T} = \frac{D_{tR}}{D_{tT}}\,, \tag{3b}$$

where τ_c is the spin probe motional correlation time; ξ_1 and ξ_o are the friction coefficients for the spin probe and the monomer unit; D_t, D_r are the diffusion coefficients for translational diffusion of the monomer unit and rotational motions of the spin probe; and the subscripts T and R refer to the corresponding values at temperatures T and T_R, respectively.

We might expect α_T' to have the same functional relationship to τ_c as α_T has to $[\tau]_T$. Hence, on substituting Equation (3a) into Equation (2a) and rearranging, one obtains the following modified form for the WLF equation

$$1/\ln(\tau_c/\tau_{cR}) = f_R^{\,2}/\{B\beta_R(T - T_R)\} + f_R/B. \tag{4}$$

The appropriate values for TEMPENE (A_{zz} = 3.50 mT, $A_{xx} = A_{yy}$ = 0.45 mT) were substituted in Equation (2) to obtain the values of τ_c as a function of temperature. These values are plotted in the form $\ln(\tau_c/\tau_{cR})$ versus $1/(T - T_R)$ and are shown in Figure 13. The linearity indicates that the modified form of the WLF equation (Equation (4)) is obeyed. The same values are also plotted in the form log τ_c versus 1/T in Figure 14, and the experimental points show a slightly curved deviation from linearity.

When a polymer is uniformly plasticized with a low-molecular-weight solvent that is molecularly dispersed (i.e., no clustering), the monomeric friction coefficients and hence the viscoelastic relaxation times are reduced.[18] The dependence of these relaxation times on the amount of solvent in the polymer is usually given by the Fujita-Doolittle equation which can be written in the form[18,20]

$$\ln \alpha_c = -\frac{(v_1 - v_1^{\,o})}{f_2^{\,o}\left[(f_2^{\,o}/\beta') + v_1 - v_1^{\,o}\right]} \tag{5a}$$

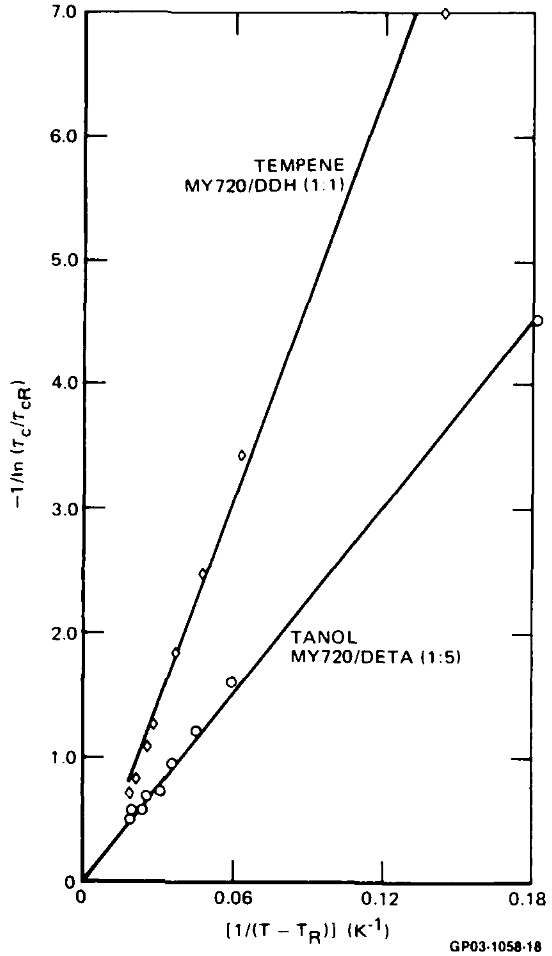

Figure 13. The WLF plots for the spin probe TEMPENE in MY720 cured with DDH (1:1 stoichiometry) and the spin probe TANOL in MY720 cured with DETA (1:5 stoichiometry).

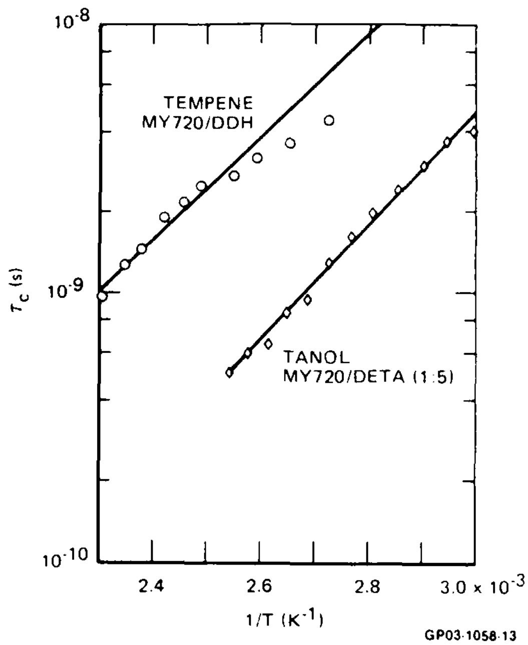

Figure 14. Motional correlation time as a function of temperature for the spin probe TEMPENE in MY720 cured with DDH (1:1 stoichiometry) and the spin probe TANOL in MY720 cured with DETA (1:5 stoichiometry).

with

$$\alpha_c = \frac{[\tau]_c}{[\tau]_R} , \tag{5b}$$

where $[\tau]_c$ is the viscoelastic relaxation time for the sample containing the solvent fraction v_1; $[\tau]_R$ and v_1^o are the corresponding values for the reference state and f_2^o and β' are constants for a given polymer/solvent system corresponding to the free-volume fraction in the reference state and the proportionality constant for the dependence of the total fractional free volume, f, on the solvent volume fraction, i.e., $f = \beta'(v_1 - v_1^o) + f_2^o$ respectively.

Again we assume that the rotational diffusion coefficient for the spin probe (or spin label) bears the same relationship to the free volume as does the monomeric translational diffusion coefficient in the polymer,[18] i.e.,

$$\alpha'_c = \frac{\tau_c}{\tau_{cR}} = \frac{[\xi_1]_c}{[\xi_1]_R} = \frac{D_{rR}}{D_{rc}} , \tag{6a}$$

whereas

$$\alpha_c = \frac{[\tau]_c}{[\tau]_R} = \frac{[\xi_o]_c}{[\xi_o]_R} = \frac{D_{tR}}{D_{tc}} , \tag{6b}$$

where the symbols are as defined in Equation (4) but the subscripts c and R refer to the values at solvent volume fractions v_1 and a reference v_1^o, respectively. Substituting Equation (6a) in Equation (5a), one obtains

$$- 1/\ln(\tau_c/\tau_{cR}) = \frac{f_2^o}{\beta'} \left[\frac{f_2^o}{(v_1 - v_1^o)} + \beta' \right] . \tag{7}$$

The temperature dependence of the spectral lineshapes for dry samples of MY720/DDH containing TEMPENE (Figure 12), where only one motional correlation time was associated with each temperature, was in marked contrast to the spectral behavior of the samples observed at room temperature on increasing the solvent content (see Figure 15). At low solvent contents (< 5 wt% methylene chloride), the spectra of the spin probe TEMPENE were only slightly modified from those of the dry samples by the presence of the solvent. At high solvent content (> 30 wt% methylene chloride), only a narrow three-line spectrum was observed. At intermediate solvent content (5 to 30 wt%), the observed spectra consisted of a superposition of a slow-phase spectrum, differing little from that of the dry sample, and a fast-phase spectrum characterized by a motional correlation time which was over one and a half orders of magnitude faster.

The spectra were digitized and stored on magnetic tape using the data acquisition system (Varian E-900). The spectra can be scaled, field-shifted, added, subtracted from one another, or integrated using the available software. The fractional amount of fast phase present in the composite spectrum was determined by removing the contribution of the slow-phase spectrum. This procedure was carried out by subtracting a scaled version of

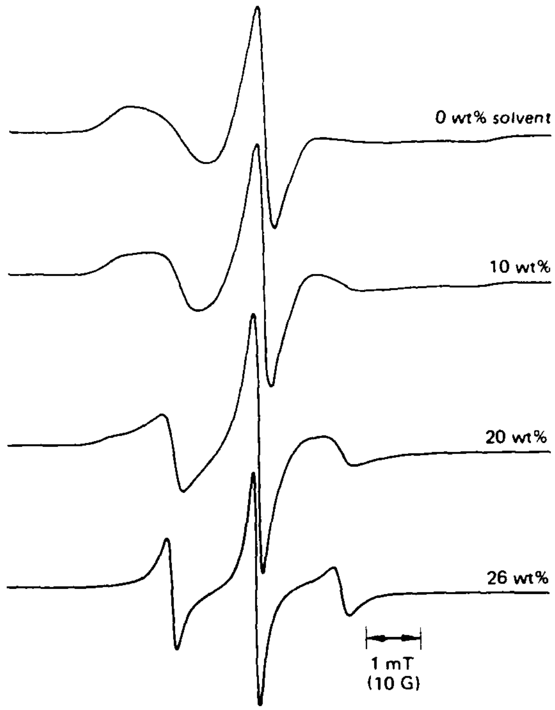

Figure 15. The effect of solvent (methylene chloride) on the EPR lineshapes for the spin probe TEMPENE in MY720 cured with DDH (1:1 stoichiometry).

the dry-sample spectrum from the composite spectrum. The best criterion for the amount to be subtracted, i.e., the scaling factor to be used, was found by displaying the resulting difference spectrum and obtaining the lineshape that appeared to be the best fit to a fast-phase spectrum. This difference spectrum and the composite spectrum were integrated, and the ratio of the areas under the integrals (i.e., the areas under the absorption spectra) was taken as the fractional amount of fast phase present. Typical examples of the composite spectrum, the dry-sample spectrum, and the resulting difference spectrum for the fast phase are shown in Figures 16a, b, and c respectively.

The spectra in Figure 15 for samples of MY720 cured with DDH containing TEMPENE and different amounts of solvent show two notable features: (a) the amount of fast phase increases with increasing solvent content, and (b) the fast-phase spectrum narrows with increasing solvent content, i.e., the motional correlation time decreases with increasing solvent content.

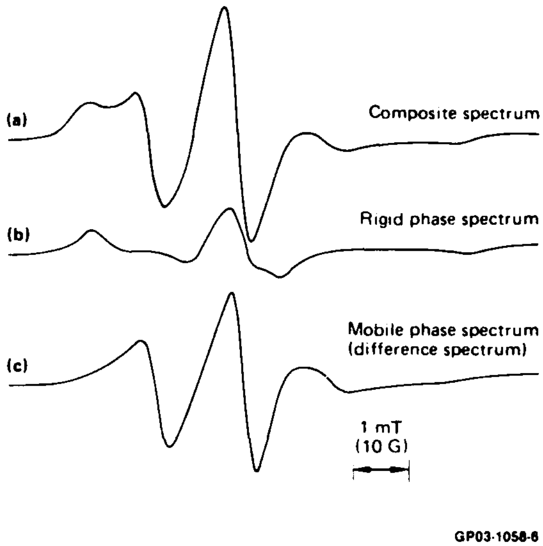

Figure 16. Typical examples of (a) the composite spectrum, (b) the dry sample spectrum, and (c) the resulting difference spectrum which is that of the fast phase.

The data plotted in Figure 17 show that the fractional amount of fast phase present is linearly dependent on solvent content from 4 to 20 wt% solvent.

The values of τ_c for the fast-phase spectrum were obtained from the line intensities using Equation (1), and the plot in Figure 18 indicates that the modified form of the Fujita-Doolittle equation shown in Equation (7) is obeyed.

Similar results were obtained with samples of MY720 cured with DDH containing the spin probe TANOL. Thus, in the temperature dependence of the EPR spectra shown in Figure 19, all spectra can be characterized by one value of the motional correlation time. On the other hand, the spectra shown in Figure 20, which were recorded as a function of solvent content, can be resolved into two components, viz., a slow-phase spectrum and a fast-phase spectrum.

The fractional amount of fast phase present, which was evaluated from the areas under the integrals of the absorption spectra (second integral of recorded spectrum), is shown as a function of solvent content in Figure 21.

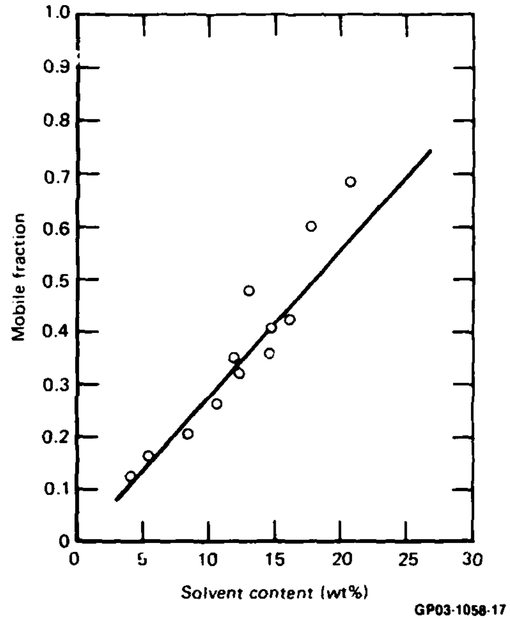

Figure 17. Mobile fraction (fast-phase content) as a function of solvent amount for a sample of MY720 cured with DDH (1:1 stoichiometry) containing TEMPENE.

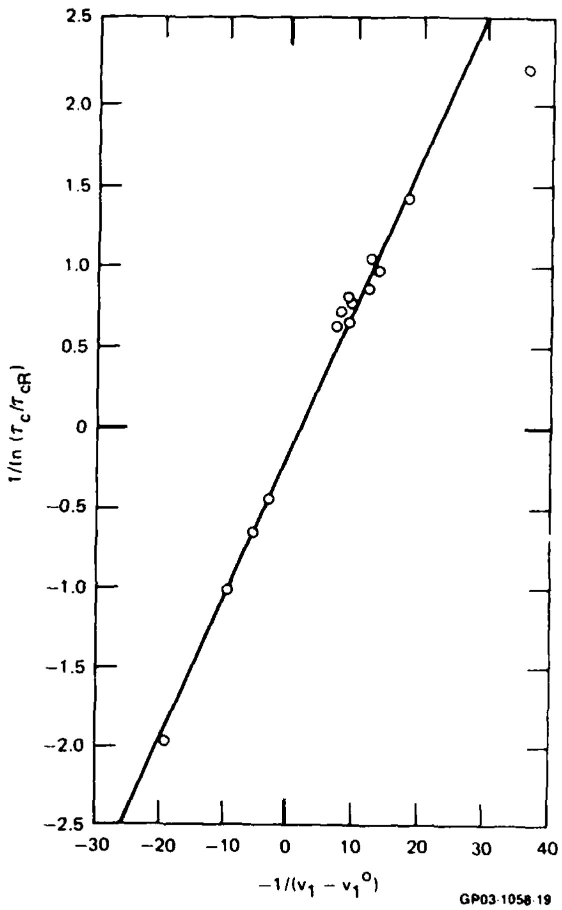

Figure 18. The Fujita-Doolittle plot for a sample of MY720 cured with DDH (1:1 stoichiometry) containing TEMPENE plasticized with methylene chloride.

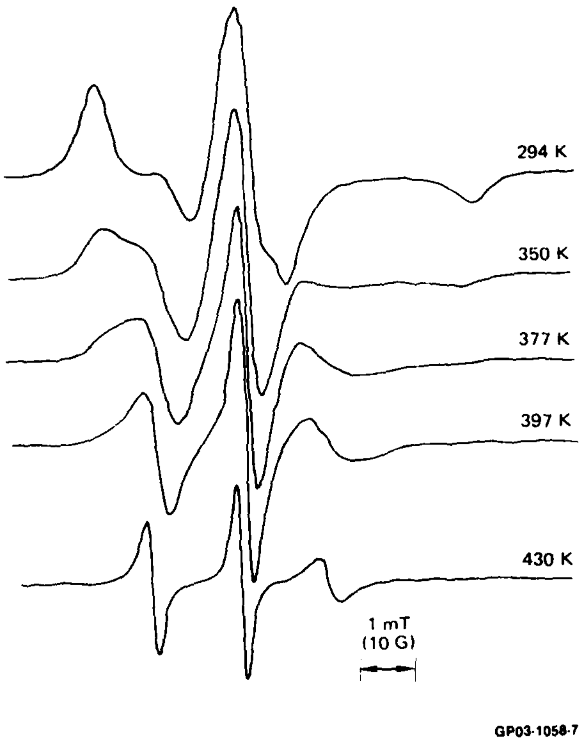

Figure 19. The temperature dependence of the EPR spectra for the spin probe TANOL in samples of MY720 cured with DDH (1:1 stoichiometry).

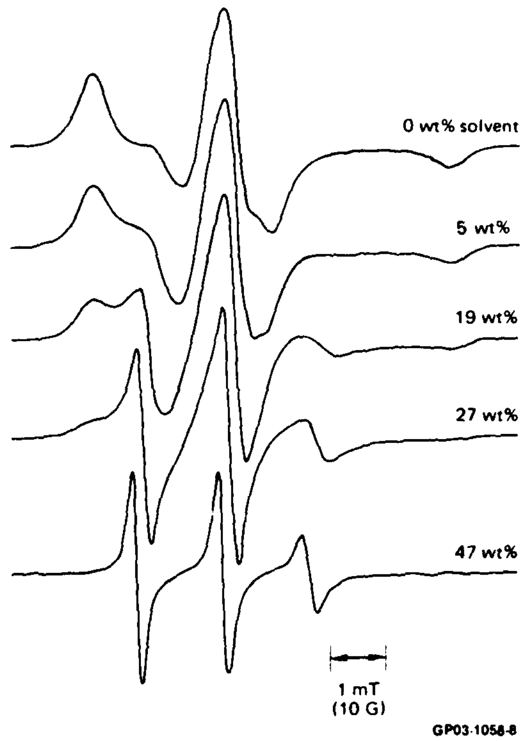

Figure 20. The effect of solvent (methylene chloride) on the EPR lineshapes for the spin probe TANOL in samples of MY720 cured with DDH (1:1 stoichiometry).

Figure 21. Mobile fraction (fast-phase content) as a function of solvent amount (methylene chloride). Samples were MY720 cured with DDH (1:1 stoichiometry) containing the spin probe TANOL.

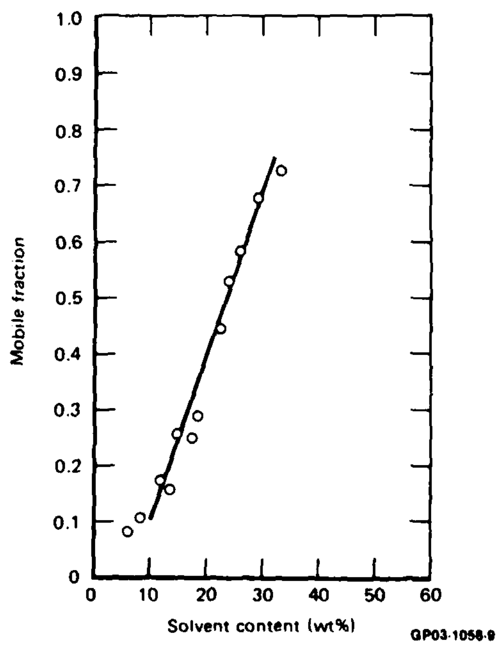

The data show an excellent fit to a linear dependence on solvent content. The linearity of the corresponding Fujita-Doolittle plot shown in Figure 22 implies that Equation (7) is obeyed.

These measurements were repeated for the spin-labeled quaternary base which formed in the reaction of DGEBA and PYRODDH at 363 K over a 48 h period (see Section 2.2). A sample of DGEBA containing small amounts of the spin-labeled quaternary base of DGEBA and PYRODDH was cured at 293 K with a stoichiometric amount of DDH. The temperature dependence of the EPR lineshapes of this cured sample was studied from 293 K to 448 K. The lineshapes showed the features typical of the onset of motional collapse and line narrowing but, again, at all temperatures the lineshapes could be characterized by a narrow distribution of motional correlation times (see Figure 23). This behavior contrasts with the results obtained with the same samples containing different amounts of the plasticizing solvent methylene chloride (see Figure 24).

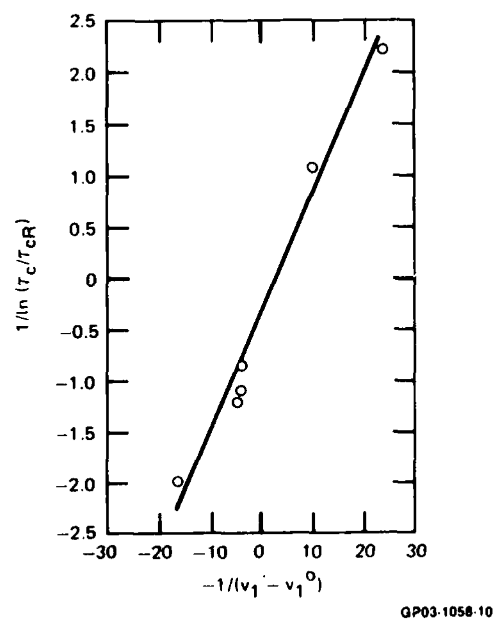

Figure 22. The Fujita-Doolittle plot for samples of MY720 cured with DDH (1:1 stoichiometry) containing the spin probe TANOL and the solvent methylene chloride.

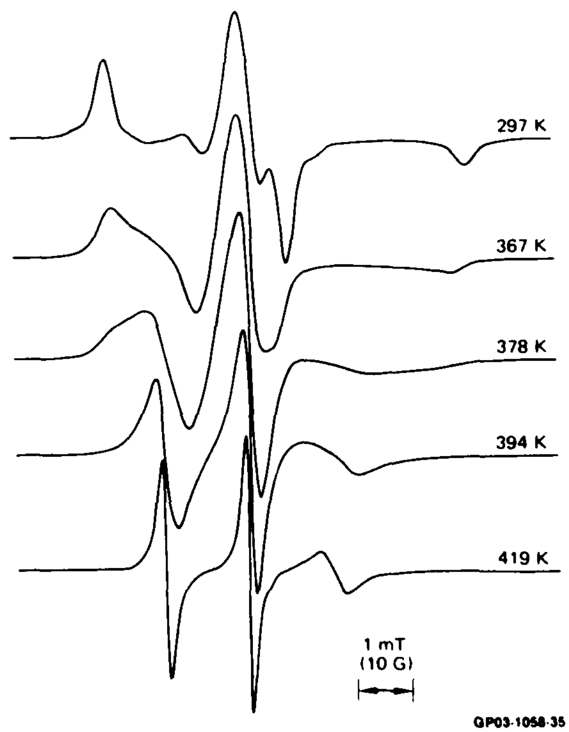

Figure 23. Temperature dependence of the EPR lineshapes for the spin label PYRODDH in samples of DGEBA cured with DDH (1:1 stoichiometry).

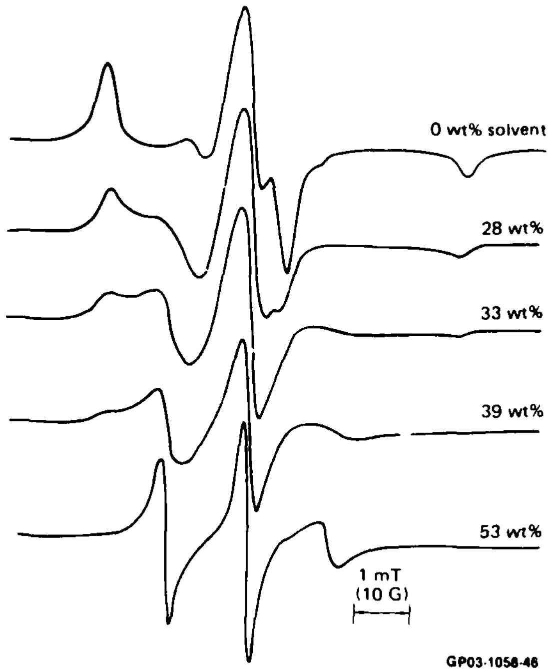

Figure 24. The effect of solvent (methylene chloride) on the EPR lineshapes for the spin label PYRODDH in samples of DGEBA cured with DDH (1:1 stoichiometry).

At low solvent content (< 15 vol%), the spectrum of the spin label was modified only slightly from that obtained in the dry polymer. At high solvent content (> 40 vol%), a motionally narrowed three-line spectrum was observed. At intermediate solvent content (15 to 40 vol%), the observed spectra consisted of a superposition of a slow phase and a fast phase. The fractional amount of fast phase present in the composite spectrum was determined by removing the contribution of the slow-phase spectrum. This procedure was performed using the data acquisition system and is described above. The plot shown in Figure 25 indicates that the fractional amount of fast phase is linearly dependent on the volume fraction of solvent from 18 to 35 vol% solvent.

The behavior of the linewidth in the fast phase indicates that the motional correlation time τ_c decreases with increasing solvent content. The values of τ_c were evaluated using Equation (1a) assuming the theory of Kivelson.[10] The plot of τ_c values versus solvent volume fraction in Figure 26 implies that the Fujita-Doolittle equation (Equation (7)) is obeyed.

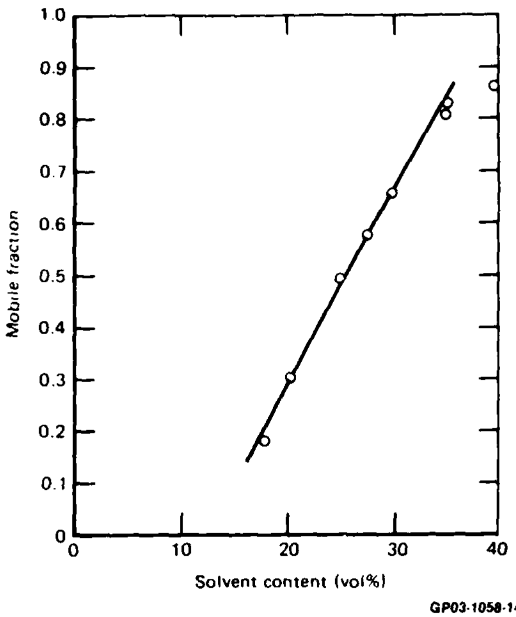

Figure 25. Mobile fraction (fast-phase content) as a function of solvent content (methylene chloride) for a sample of DGEBA cured with DDH (1:1 stoichiometry) and labeled with PYRODDH.

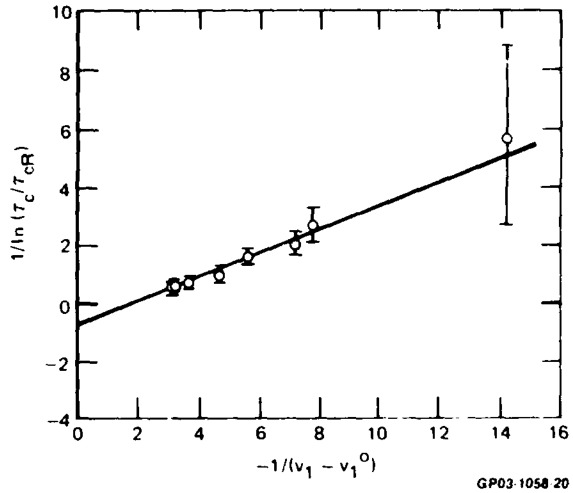

Figure 26. The Fujita-Doolittle plot for samples of DGEBA cured with DDH (1:1 stoichiometry) containing the spin label PYRODDH and the solvent methylene chloride.

Spin label studies in cured samples of MY720 could not be pursued because the nitroxide EPR signal decreased by over one order of magnitude before the label formed. This decrease is due to nitroxide decomposition and is described in more detail in Section 2.2.

A series of similar experiments was performed in epoxy samples which were plasticized with water. The spin probe TANOL was dissolved in the uncured epoxy resins DGEBA and MY720 which were then cured with nonstoichiometric amounts of DETA. The stoichiometric ratios were DGEBA:DETA = 1:3 and MY720:DETA = 1:5. Excess DETA was used in the cures to allow the sorption of large amounts of water (> 4 wt%). As shown in Figures 27 and 28, at low water content (< 7 wt% in DGEBA/DETA and < 1 wt% in MY720/DETA), the spectra of TANOL were modified only slightly from those of the dry samples. At higher water content (7 to 32 wt% in DGEBA/DETA and 1 to 25 wt% in MY720/DETA), the observed spectra consisted of a superposition of a slow phase and a fast phase. The maximum water content was never high enough to produce a spectrum which was 100% fast phase.

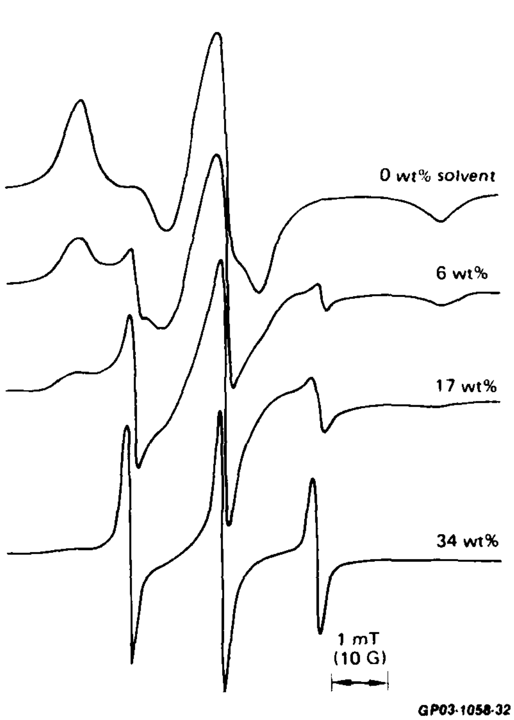

Figure 27. The effect of solvent (water) on the EPR lineshapes for the spin probe TANOL in DGEBA cured with DETA (1:3 stoichiometry).

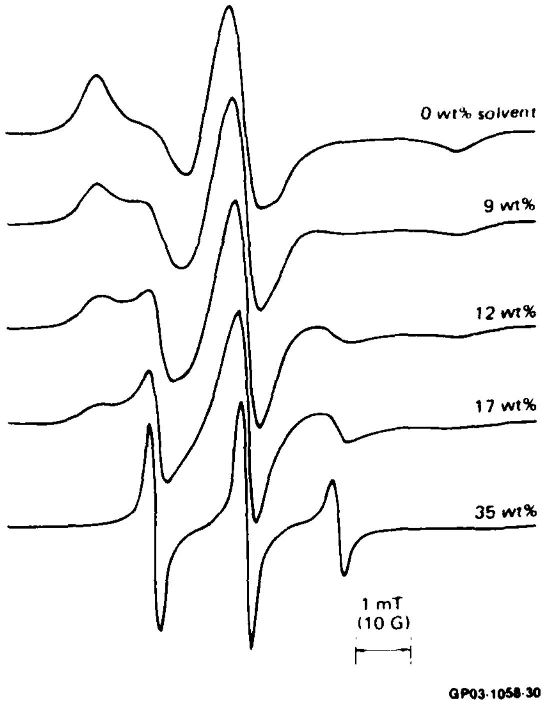

Figure 28. The effect of solvent (water) on the EPR lineshapes for the spin probe TANOL in samples of MY720 cured with DETA (1:5 stoichiometry).

The plot shown in Figure 29 for DGEBA/DETA indicates that the fractional amount of fast phase is linearly dependent on the water content from 7 to 34 wt% water, whereas the plot in Figure 30 for MY720/DETA indicates a linear dependence for the fast-phase fraction on water content from 1 to 25 wt% water.

The behavior of the EPR spectra of TANOL in the fast phases in both cured resin systems indicates that the motional correlation time τ_c decreases with increasing water content. The values of τ_c were evaluated from Equation (1). The plots of the τ_c values shown in Figures 31 and 32 indicate that the Fujita-Doolittle equation (Equation (7)) is obeyed.

The temperature dependence of the EPR lineshapes for TANOL in both DGEBA/DETA and MY720/DETA dry samples (see Figure 33) indicates that at all temperatures, the spectral lineshapes can be characterized by one value of the motional correlation time. Values of τ_c for TANOL in the MY720/DETA samples were evaluated from Equation (1). These values are plotted in Figures 13 and 14 where they show an excellent fit to both the WLF equation (Equation (4)) and to an exp(E/RT) relationship with E = 41 kJ mole^{-1}.

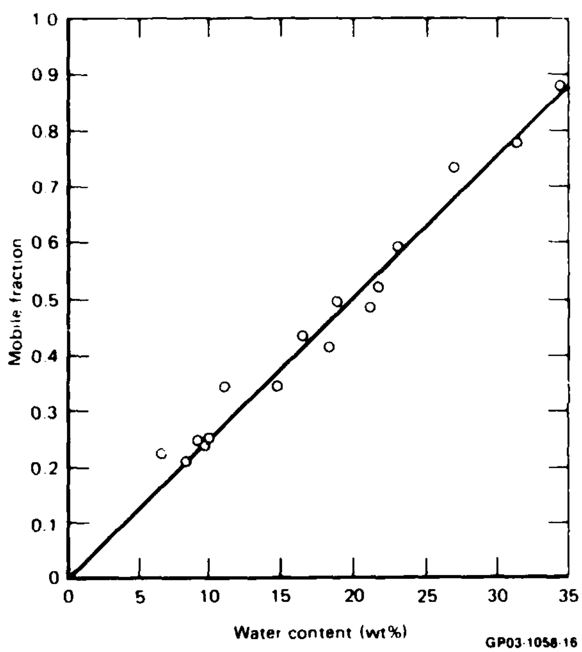

Figure 29. Mobile fraction (fast-phase content) as a function of water content (wt%) for samples of DGEBA cured with DETA (1:3 stoichiometry) containing the spin probe TANOL.

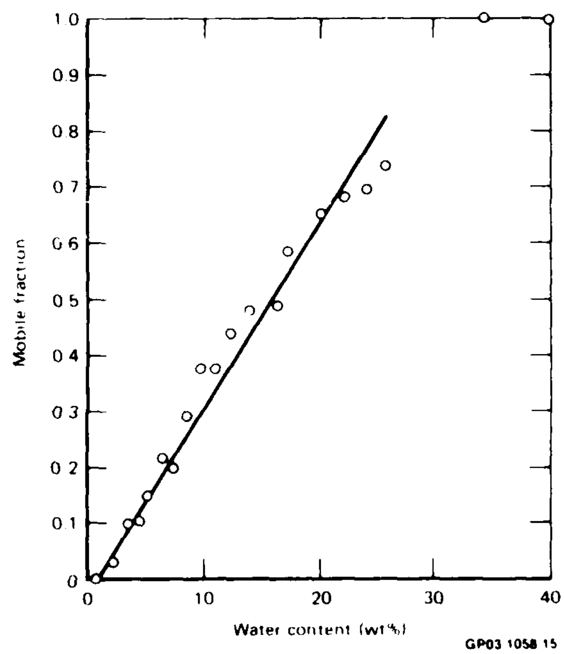

Figure 30. Mobile fraction (fast-phase content) as a function of water content (wt%) for samples of MY720 cured with DETA (1:5 stoichiometry) containing the spin probe TANOL.

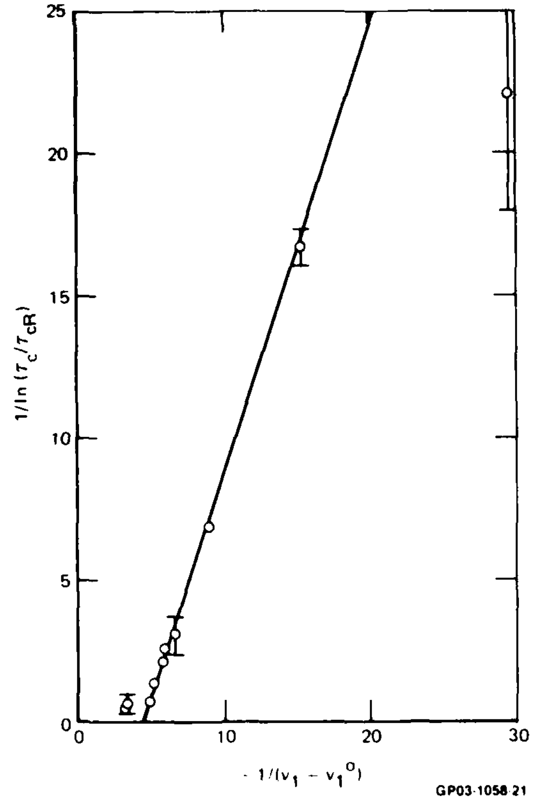

Figure 31. Fujita-Doolittle plot for samples of DGEBA cured with DETA (1:3 stoichiometry) containing the spin probe TANOL and the solvent water.

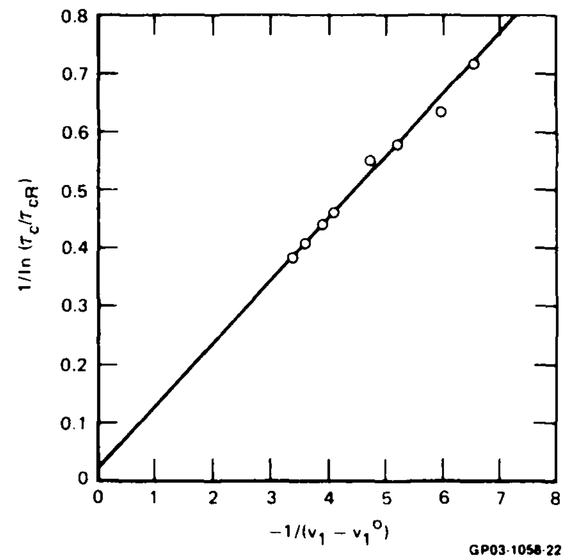

Figure 32. Fujita-Doolittle plot for samples of MY720 cured with DETA (1:5 stoichiometry) containing the spin probe TANOL and the solvent water.

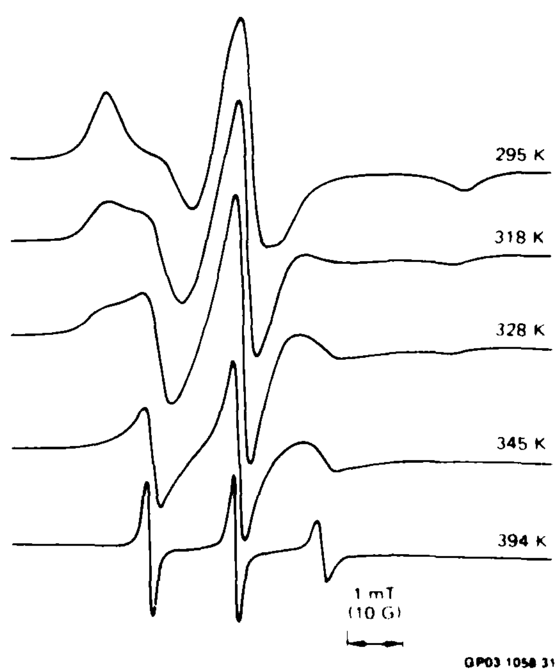

Figure 33. Temperature dependence of the EPR lineshapes for the spin probe TANOL in samples of MY720 cured with DETA (1:5 stoichiometry).

2.4 Discussion of EPR Results

The EPR results described in Section 2.3 will be interpreted in terms of the polymer microstructure that is present because of the inhomogeneities in crosslink density in the network. An acceptable model for the network morphology must explain the following major experimental findings:

1. the fit of the temperature-dependent data to the WLF equation,
2. the fit of the solvent-dependent data to the Fujita-Doolittle equation,
3. the presence of only one spectrum at each temperature in the dry sample, and
4. the superposition of two spectra in samples plasticized with either water or methylene chloride.

As is illustrated in Figures 13 and 14, an analysis of the temperature dependence of the data for TANOL in MY720/DETA (1:5 stoichiometry) shows that the motional correlation times in the fast regime can be fitted to either the modified WLF equation (Equation (4)) or the Arrhenius equation. The reason for this is that the temperature range studied is sufficiently small (60 K) that the WLF equation closely approximates the Arrhenius form. If the data were taken over a wide-enough temperature range, it should be possible to distinguish between the WLF and Arrhenius form for the best fit to the data. Yet there is a limitation since it is not possible to extend the data above ~ 430 K because of nitroxide decomposition. On the other hand, as illustrated in Figures 13 and 14, the values of the motional correlation time for TEMPENE in MY720/DDH show a better fit to the WLF equation than the Arrhenius equation. Further evidence for the validity of the WLF equation describing the motion of the spin probe in the dry polymers is contained in the behavior of the spin probes in the plasticized polymer.

According to the theory of Cohen and Turnbull[21], the WLF equation can be derived assuming that molecular translational diffusion depends only on the instantaneous free-volume fluctuations adjacent to the diffusing molecule. Free volume added to the polymer by way of a plasticizing solvent should therefore affect the viscoelastic properties in a similar manner to the free-volume added by way of an increase in temperature. The corresponding relationship for samples containing plasticizing solvents, which is derived assuming free volume changes only, is the Fujita-Doolittle equation (Equation (5)).

As described in Section 2.3, in the five samples plasticized with either water or methylene chloride, the behavior of the motional correlation times for the fast phases shows excellent agreement with the modified Fujita-Doolittle equation. We conclude that the agreement of the spin probe data in the dry polymers with the modified WLF equation, and the agreement of the spin probe data in the plasticized polymer with the modified Fujita-Doolittle equation indicate that the motion of the spin probe is sensitive to free volume in the polymer. The question to be answered is why only one spectrum is observed at each temperature in the dry sample, but two spectra are observed at many solvent contents in the plasticized polymers.

These results can be reformulated in the following manner: the onset of the motional narrowing of the EPR lineshapes can be crudely characterized by a temperature range δ_T and a critical temperature T_C. These definitions are illustrated in Figure 34 which depicts the typical form of the temperature dependence of the extrema splitting for a set of spin probes in identical environments in the polymer. Thus the value of δ_T is determined by the range of temperatures over which the motional narrowing occurs, whereas the value of T_c is determined by the temperature above which the motional correlation time is in the fast motion regime, i.e., $\tau_c \lesssim 10^{-9}$ s. Although T_C may not correspond to T_g, it usually is related to it because the spin probe motion is sensitive to changes in free volume and hence to the onset of the segmental motions. A distribution in crosslink density implies that the spin probes in regions with different rigidities will exhibit different values of T_C, e.g.,

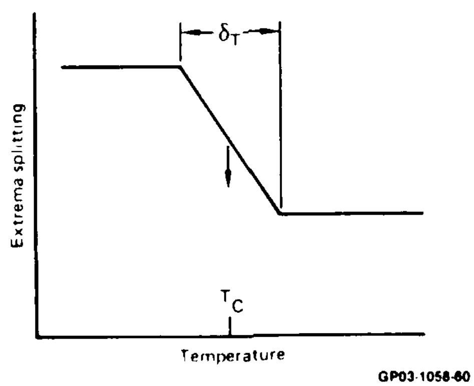

Figure 34. Idealized temperature dependence of extrema splitting; δ_T is the temperature range over which the motional correlation time goes from the slow (10^{-7}s) to the fast (10^{-11}s) extremes. T_C is the critical temperature.

T_{C1}, T_{C2} in Figure 35. Thus, a distribution in crosslink density results in a distribution in T_C values which can be characterized by a half-width Δ_T. The temperature dependences of the EPR lineshapes described in Section 2.3 indicate only a narrow distribution of motional correlation times at a given temperature. These results therefore imply that the relation $\Delta_T/\delta_T < 1$ holds.

The solvent dependence of the EPR lineshapes can be characterized in an analogous manner, i.e., the motional correlation time will be in the fast motional regime for samples with solvent contents above a critical value v_C. Moreover, low crosslink regions will be plasticized at low solvent contents so that the value of v_C in those regions (e.g., v_{C1} in Figure 35) will be less than that in a higher crosslink region (v_{C2} in Figure 35). In other words, a

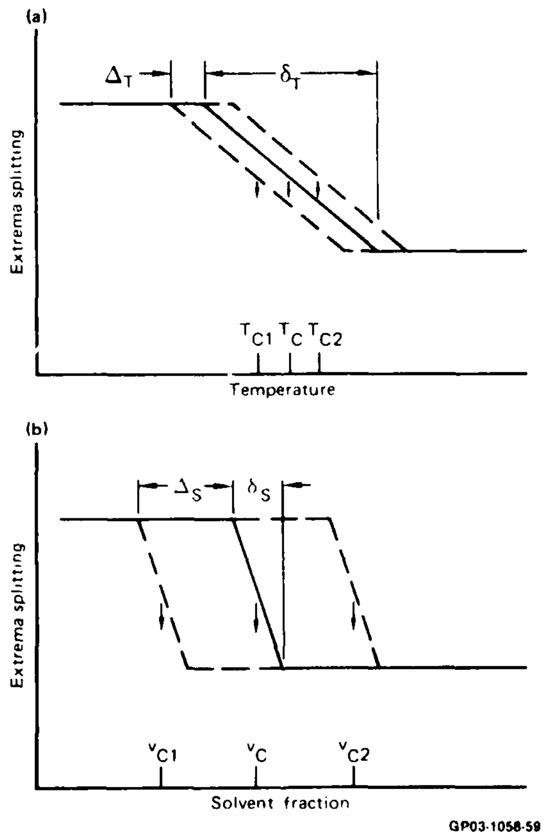

Figure 35. (a) Idealized temperature dependence of the extrema splitting when there is a distribution of critical temperatures $T_{C1},...T_{C2}$ with a half-width Δ_T, and (b) idealized solvent dependence of the extrema splitting when there is a distribution of critical solvent fractions $v_{C1}, ...v_{C2}$ with a half-width Δ_S.

distribution in crosslink density will produce a distribution in v_C values with half-width Δ_S. The results in Section 2.3, where a bimodal distribution of correlation times differing by one and a half orders of magnitude was observed on addition of the low molecular weight plasticizing solvent, indicate a wide range of correlation times. These results imply that the relation $\Delta_S/\delta_S \gtrsim 1$ holds.

We have shown in Appendix A that for samples with the same free volume content,

$$\frac{\Delta_T}{\delta_T} = \frac{\Delta_S}{\delta_S} \; . \tag{8}$$

It is difficult to reconcile Equation (8) with the conclusions described above which were drawn from the experimental results except in the following manner. In Appendix A it was assumed that the solvent was dispersed uniformly and the plasticization was nonuniform only in as much as the rigid regions (more dense crosslinking) become rubbery at higher solvent contents than the less rigid regions. The EPR results indicate that the temperature dependent and solvent dependent results are different in nature. We therefore conclude that the solvent preferentially partitions into the low crosslinked regions. As a result, the low crosslink regions, which have the greatest free volume in the dry polymer, have even greater free volume content following addition of the solvent. The overall effect of the solvent plasticizer is to emphasize the differences in rigidity and hence spin probe mobility in the polymers so that microstructural features not observable on varying the temperature will show up on varying the solvent plasticizer content. The solvent partitioning will therefore produce an increase in Δ_S so that $\Delta_S/\delta_S \gtrsim 1$.

From the results of previous work[22,23] it might be expected that the rate for translational diffusion of the spin probes in the rubbery regions is fast. Furthermore, if the spin probes could penetrate the interphase regions between the rubbery and rigid regions, the temperature dependent equilibrium of numbers in the fast and slow phases would determine the spectral lineshapes. The EPR experiments were repeated for the spin label PYRODDH which is prevented from undergoing translational diffusion because of the constraints imposed by the covalent binding. The results shown in Figures 23 and 24 are the same as those for the spin probe, implying that the translational diffusion of the spin probe has a minor role in determining the EPR lineshapes.

The spin probes go from the slow to the fast phase by the boundary defining the rigid and rubbery regions moving past the probe site. The motion determining the value of the correlation time for the spin probe is rotational motion at a fixed site.[22,23]

The number of spin probes undergoing fast motion, which is given by the area under the fast phase EPR spectrum, is then a measure of the amount of rubbery region present. It is not obvious from our model, however, that the mobile fraction should be linearly dependent on the solvent content.

If $p(v_o - v_C)$, the probability function for the distribution of v_C values, has a Gaussian form, then it can be written

$$p(v_o - v_C) = \exp\left[- \frac{(v_o - v_C)^2}{\Delta_S^2}\right] , \tag{9}$$

where v_o is the center of the distribution and Δ_S is the half-width.

The mobile fraction f is then given by[23]

$$f = \Lambda \int_{-\infty}^{v_C} p(v_o - v_C)\,dv_C \tag{10a}$$

$$= \frac{1}{2}\left(1 \mp \mathrm{erf}[(v_o - v_C)/\Delta_S]\right) , \tag{10b}$$

where Λ is the normalization constant.

A distribution in rigidities arising from a variation in crosslink density is incorporated through the Gaussian probability function. The solvent partitioning among the regions with different rigidities can be included by allowing Δ_S to be a function of solvent content.

We have been unable to pursue this treatment further to obtain an analytical solution but offer the following numerical calculations as an illustrative explanation of our experimental results.

We divide the sample into nine regions. The solvent partitioning into the i^{th} region is described by a parameter γ_i defined as (the volume of solvent in region i)/(the volume of solvent that would be in region i if the solvent were uniformly distributed throughout the sample). We assume that as i goes from 1 to 9, γ_i has the value $\gamma_i = 0.1(15 - i)$. The solvent volume fraction in the i^{th} region is given by $\gamma_i k/(\gamma_i k + p)$, whereas the average solvent volume fraction is $k/(k + p)$, where k is the volume of solvent added to the sample and p is the volume of dry polymer. The solid lines shown in Figure 36 are plots of solvent volume fraction in the i^{th} region as a function of the average solvent volume fraction. The dashed line in Figure 36 is the line of plasticization. The intersection of the line of plasticization with the i^{th} solid line defines the solvent volume fraction in the i^{th} region, above which the i^{th} region is plasticized and above which the spin probes in the i^{th} region are in the fast phase. Each solid line describing the solvent volume fraction in the i^{th} region is weighted with an approximate Gaussian distribution to account for a distribution in sizes of thc regions with different rigidities. We evaluated the mobile fraction in the sample

Region (i)	γ_i	Gaussian weighting factor
1	1.4	0.056
2	1.3	0.081
3	1.2	0.104
4	1.1	0.122
5	1.0	0.128
6	0.9	0.122
7	0.8	0.104
8	0.7	0.081
9	0.6	0.056

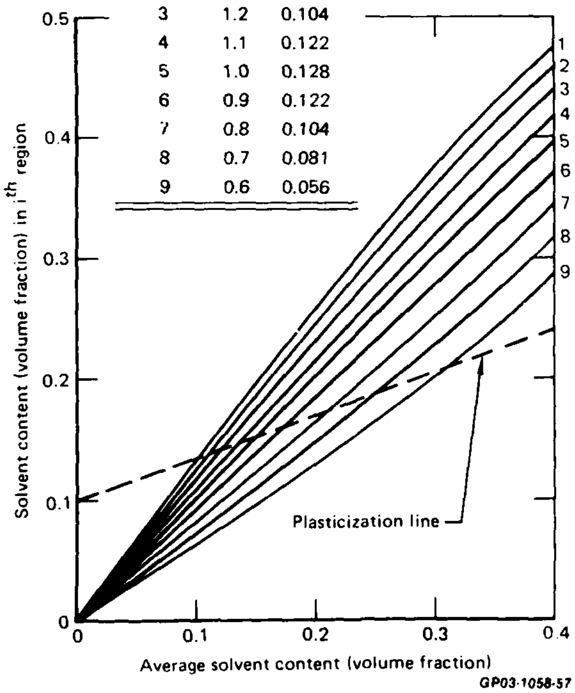

Figure 36. Solvent content (volume fraction) in the i^{th} region of the sample as a function of the average solvent content (average volume fraction) in sample. Values of γ_i and Gaussian weighting factor for each region are included. The dashed line is the plasticization line.

(fraction of spin probes in the fast phase) as a function of average solvent fraction by adding the weighted numbers of spin probes in the i^{th} regions which are above the line of plasticization. The results for different average solvent fractions are shown in Figure 37. As can be seen in Figure 37, the mobile fraction is approximately linearly dependent on average solvent fraction, which agrees with the experimental observations described in Section 2.3.

Measurements on samples of DGEBA/DDH (1:1 stoichiometry) using differential scanning calorimetry show that the glass transition can be reduced to room temperature with ≈ 5 wt% methylene chloride.[24] The value of the motional correlation time for the spin label at this solvent content (~ 10^{-8} s) is obtained by extrapolating the values deduced from Figure 38.

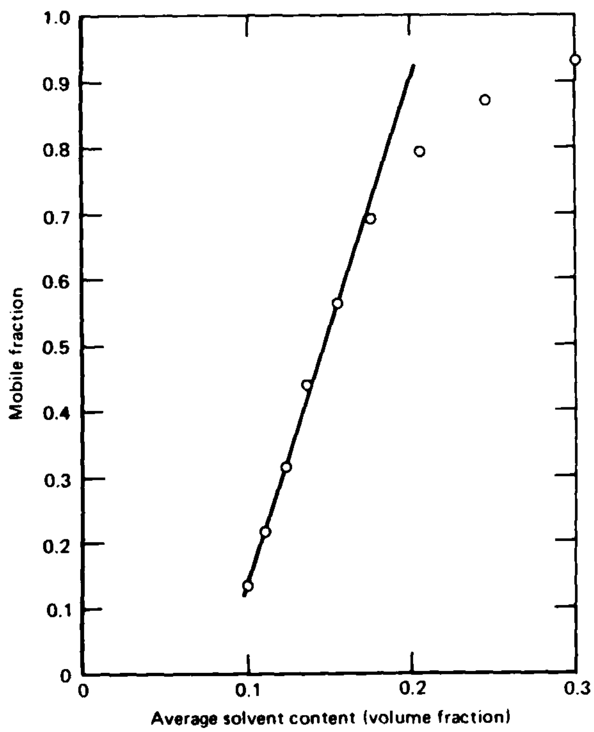

Figure 37. Mobile fraction (fast-phase content) as a function of average volume fraction of solvent present in the hypothetical nine region sample described by Fig. 36.

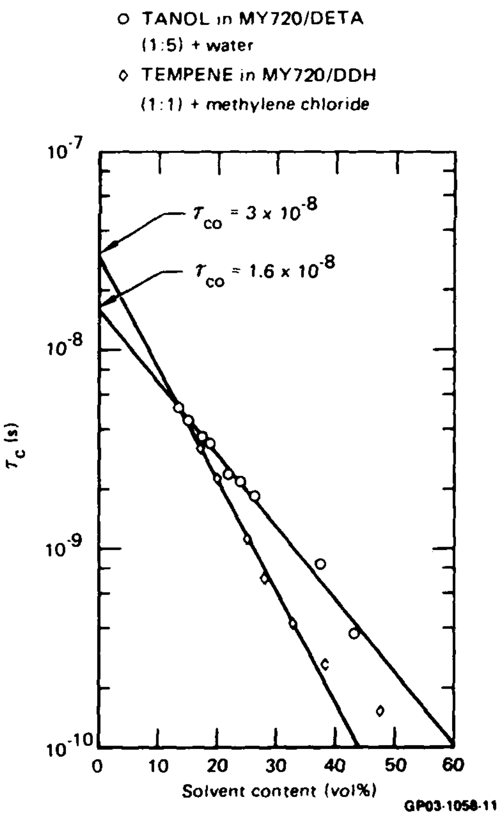

Figure 38. Motional correlation times as a function of solvent content for TANOL in MY720 cured with DETA (1:5 stoichiometry) plus water and for TEMPENE in MY720 cured with DDH (1:1 stoichiometry) plus methylene chloride.

Since this value is eight orders of magnitude faster than that associated with the main-chain segmental motions at the glass transition, we attribute the motion of the spin label to be largely due to a solvent-dependent local mode of motion located on the main-chain backbone extending only a few bonds from where the nitroxide is attached to the main chain.[25,26]

The data in Figure 38 imply that the value of the motional correlation time for TEMPENE in MY720/DDH containing 5 wt% methylene chloride is 1.5 x 10^{-8} s. However, because of the lack of covalent bonding, there are fewer constraints on the motion of the spin probe, and the correlation time for the spin probe need not be equal to that of the polymer. Thus the motions of the spin probe could be the result of either the main-chain segmental motions or local modes that precede the onset of the main-chain segmental motion.

3. NMR EXPERIMENTS

3.1 NMR Samples

Two different epoxy resins were used in this study: diglycidyl ether of bisphenol A (DGEBA) in its commercial form DER332 (Dow Chemical Company) and tetraglycidyl-4,4′-diaminodiphenyl methane (TGDDM) in its commercial form MY720 (Ciba Gergy). The DER332 was cured with N,N′-dimethyl-1,6-diaminohexane (DDH) or 1,2-cyclohexanedicarboxylic anhydride (CHCA) with tripropylamine (TPA), and the MY720 was cured with DDH. The calculated stoichiometric mixtures for the systems (based on the epoxide equivalent weights supplied by the manufacturers) were 348 g DER332 to 144 g DDH, 174 g DER332 to 154 g CHCA plus 3.3 g TPA, and 125 g MY720 to 72 g DDH. Samples made from nonstoichiometric mixtures are denoted by 1:R, where R refers to the amount of curing agent used relative to the stoichiometric amount.

All samples were made by mixing the constituents at elevated temperature to reduce the viscosity so that a homogeneous mixture could be achieved easily. The mixture was vacuum pumped to remove trapped air and was then poured into silicone rubber molds to produce 3.2 mm diameter cylindrical rods. The rods were cured for 24 h at room temperature and post cured for 24 h at 400 K. Cylinders approximately 6 mm long were cut from these rods to serve as the NMR samples.

3.2 NMR Measurements

Pulsed hydrogen NMR experiments were performed on a variable-temperature, single-coil spectrometer operating at 100 MHz. The signal from an external fluorine sample at 94 MHz was used to stabilize the magnetic field so that small signals could be signal-averaged without attending drift. The 100 MHz and 94 MHz rf signals were derived from a frequency synthesizer (Hewlett Packard HP5100). The 8 mT, pulsed, rf magnetic fields were generated using a programmable digital pulser[27] and a 100 W linear amplifier (Electronic Navigation Industries 3100L). A transient recorder (Biomation 826) in conjunction with a signal averager (Nicolet 1074) were used to collect and store data from as many as four different experiments. During the first half of the contract period, the data were analyzed in a computer able to store data from only one experiment at a time (Digital Equipment Corporation

PDP8/f). During the second half of the contract period, a computer capable of storing data from hundreds of experiments was used (Digital Equipment Corporation MINC). The latter computer permitted lengthy series of experiments to be performed in a short time period without the delays previously needed for data analysis, thus improving the quality of data obtained at high temperatures because the samples did not undergo significant changes during the short time of the experiments. Further improvements also resulted from the ability to review the raw data from an entire series of measurements at a later time and extract additional information by subjecting it to different analysis procedures.

Three different types of pulsed NMR experiments were performed: 1) a single 90^{o} pulse experiment to determine the relative amounts of rigid and mobile phases and their spin-spin relaxation times,[12] 2) a 180^{o}, τ, 90^{o} pulse experiment to determine the spin-lattice relaxation times,[12] and 3) a 90^{o}, τ_1, -90^{o}, τ, 90^{o} pulse experiment to measure the sizes of the mobile regions.[15,28] The free-induction decay signals from the above experiments were analyzed either in the time domain or in the frequency domain after Fourier transformation.

3.3 Characteristics of Epoxy Resin Polymer NMR Signals

The free-induction decay signal of a cured epoxy resin polymer contains two components, as shown in Figure 39. (The absence of a signal for small times is caused by receiver overload.) The computer performs a least squares fit to the free-induction decay signal to determine the five parameters A_G, T_{2G}, n, A_L, and T_{2L}. Unplasticized, stoichiometric epoxy resin polymers at room temperature generally contain a true Gaussian component, i.e., n = 2. In general, the Gaussian component results from hydrogen in molecules that are rigid, and the Lorentzian component results from hydrogen in molecules that are undergoing liquid-like motion. Thus, the Gaussian component results from the rigid polymer below its glass transition temperature, and the Lorentzian component results from sorbed solvents, plasticized polymer, or polymer above its glass transition temperature. The Gaussian amplitude, A_G, and the Lorentzian amplitude, A_L, are proportional to the number of hydrogen in the rigid and mobile portions of the polymer, respectively.

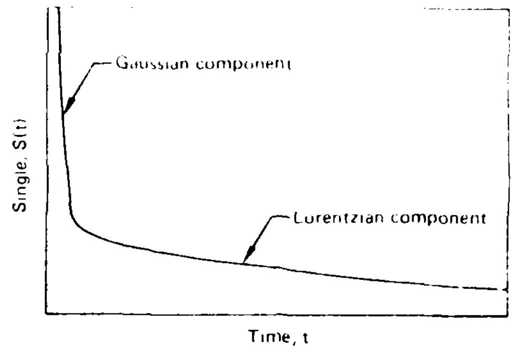

Signal = Gaussian component (rigid) + Lorentzian component (mobile)

$$S(t) = A_G \exp\left\{-(t/T_{2G})^n\right\} + A_L \exp\left\{ t/T_{2L}\right\}$$

GP03-1058-41

Figure 39. Hydrogen NMR free-induction decay signal.

3.4 Temperature-Dependent NMR Measurements of Dry Samples

Temperature-dependent NMR measurements were performed on dry samples of MY720:DDH having three different stoichiometries: 1:0.5, 1:1, and 1:2. The temperature dependence of the Lorentzian and pseudo-Gaussian spin-spin relaxation times T_{2L} and T_{2G}, and the Lorentzian fraction F_L, ($F_L = A_L/(A_L + A_G)$), are plotted in Figures 40 and 41, respectively for the three different sets of samples. The increase in the T_2's and F_L's with increasing temperature is a result of increased molecular motion at the glass transition temperature. Generally, when the correlation time for the motion of a molecular group becomes less than its spin-spin relaxation time, the spin-spin relaxation time increases abruptly. Because there are a number of different molecular groups in cured epoxies with different mobilities and because their motion is generally anisotropic, an abrupt increase in T_{2G} was not observed. The T_{2G} data show that 1) the onset of the increase occurred at lower temperatures and 2) the increase reached a plateau at higher values for samples with larger DDH contents. These observations suggest that the excess DDH produces lightly crosslinked regions in which 1) the onset of extensive molecular motion occurs at low temperatures and 2) the motion is much less restricted (more isotropic) above the glass transition.

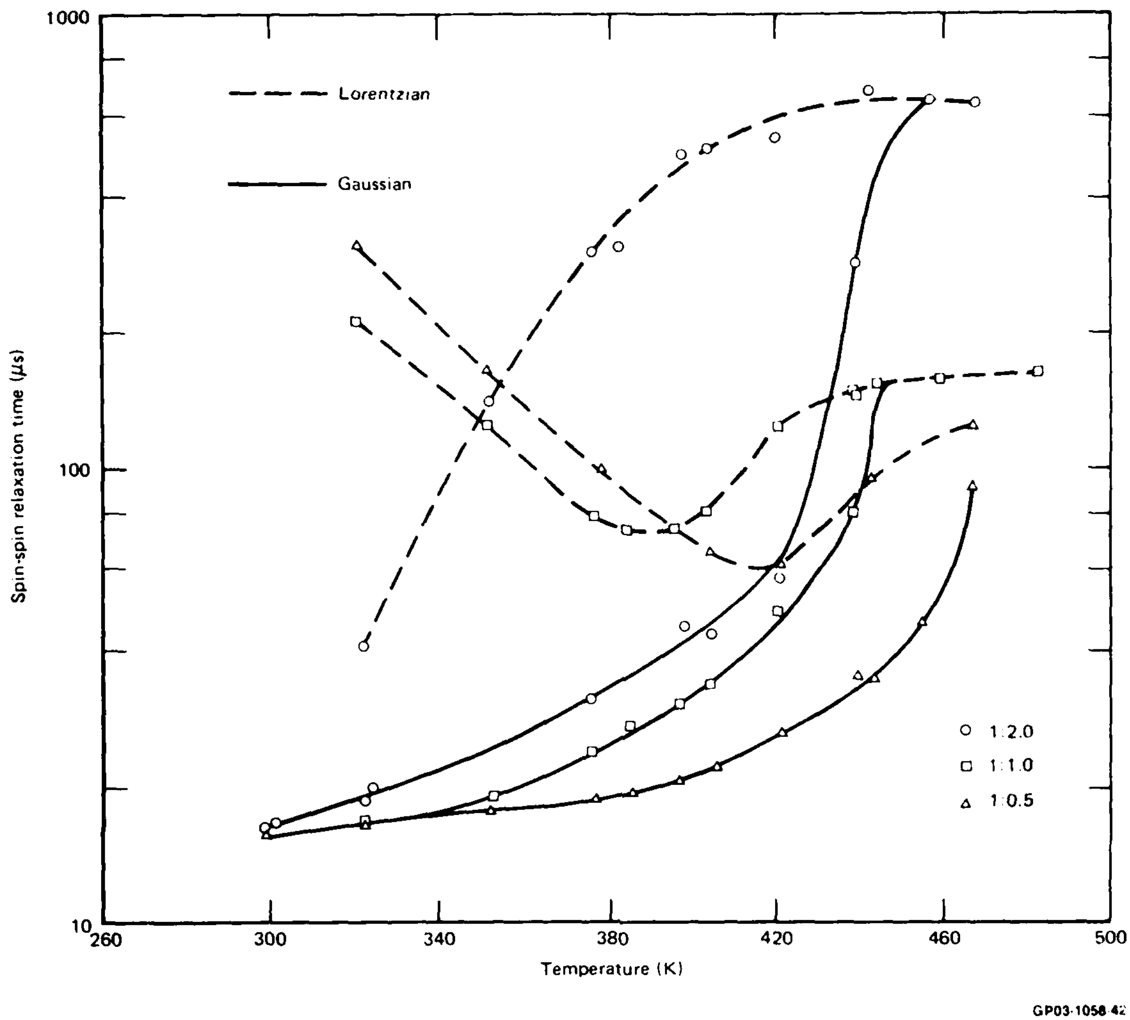

Figure 40. Temperature dependence of the spin-spin relaxation times for MY720:DDH samples having different stoichiometries.

The significance of the value of T_{2L} at the plateau is important and deserves additional discussion. Below the glass transition, T_{2L} and T_{2G} approach a common limit. If the molecular motion were unrestricted so that isotropic tumbling could occur, T_{2L} would continue to increase with increasing temperature. The limiting value at the plateau is an indication of the amount of restriction to molecular motion, which reflects the degree of crosslinking. Thus, the 1:0.5 sample has the greatest crosslinking; the 1:2 sample has the least. The 1:0.5 sample undoubtedly has undergone homopolymerization via ether links initiated by tertiary amines. These short ether links create a crosslink structure that is less mobile than that

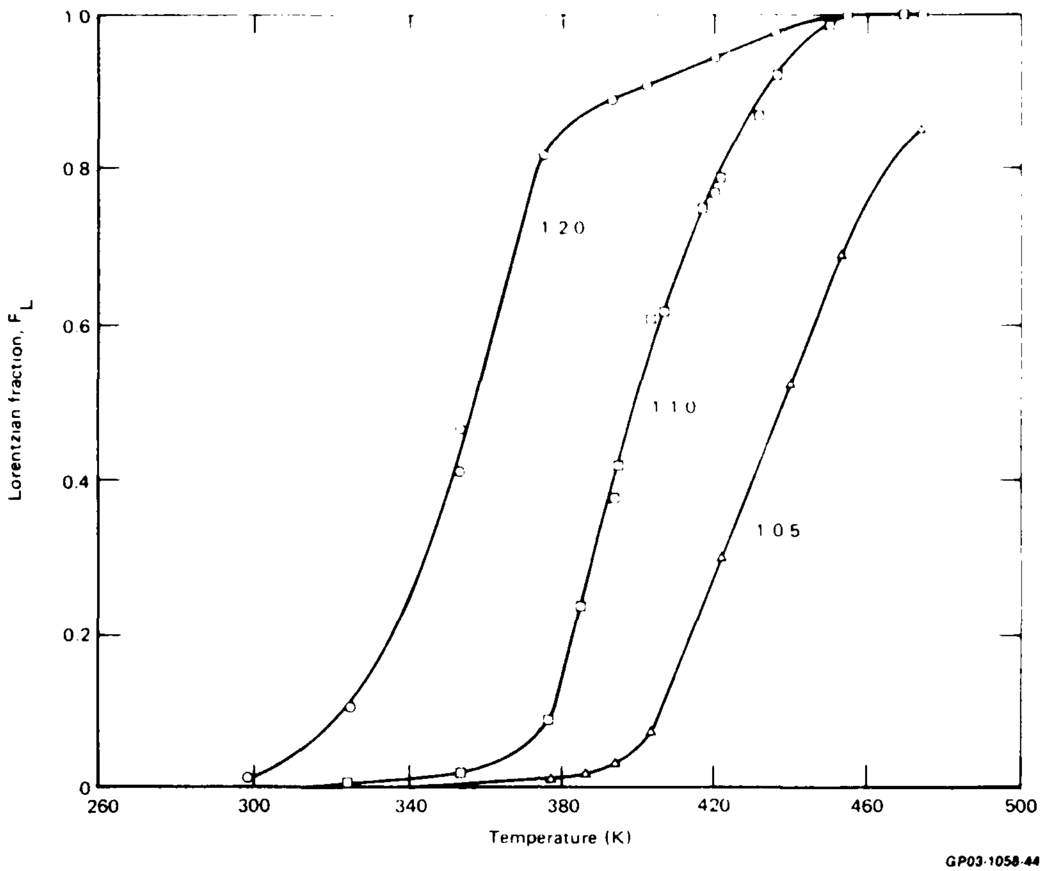

Figure 41. Temperature dependence of the Lorentzian fraction for MY720:DDH samples having different stoichiometries.

produced by the much longer DDH links. Hence, the 1:0.5 sample has a higher glass transition temperature and smaller mobility above the transition temperature than the 1:1 or 1:2 samples.

The Lorentzian spin-spin relaxation times for the 1:0.5 and 1:1 samples decrease with increasing temperature between 320 K and ≈ 390 K. These results are misleading and are best understood by referring to the Lorentzian fraction data shown in Figure 41. Below ≈ 390 K only a small fraction of the signal was Lorentzian, but it was slowly increasing. The T_{2L} data are interpreted as the result of a small-amplitude Lorentzian signal with a large T_{2L} being masked by a second Lorentzian signal with a smaller T_{2L} as the amplitude of the second Lorentzian signal increased with increasing temperature. The origin of the small amplitude Lorentzian signal with a large T_{2L} could have been sorbed water or unreacted DDH. The origin of the second Lorentzian signal with the smaller T_{2L} was probably rigid epoxy becoming sufficiently mobile with increasing temperature that its Gaussian character became Lorentzian.

Below the glass transition temperature, the pseudo-Gaussian relaxation, $A_G \exp\{-(t/T_{2G})^n\}$, had n = 2. As the temperature increased through the glass transition, n gradually decreased from 2 to 1. When n = 1, the relaxation times of the Lorentzian and pseudo-Gaussian became equal and the relaxation was totally Lorentzian, i.e., $F_L = 1$.

The T_{2L} and F_L data for the 1:2 sample show that the excess DDH produced a sizable Lorentzian component just above 320 K. Thus, in addition to the excess DDH producing a lightly crosslinked network, it also plasticized the sample at a relatively low temperature to produce a large mobile fraction F_L.

The temperature dependence of the Lorentzian fraction F_L shows more clearly the onset of the glass transition than does the spin-spin relaxation time T_2. In a crosslinked system such as this, one could define the onset of the glass transition as the temperature at which a straight line through the measured F_L data intersects the temperature axis, and an average glass transition temperature as the temperature at which $F_L = 0.5$.

The temperature dependence of the spin-lattice relaxation times T_1 are plotted in Figure 42 for the MY720:DDH samples having three different stoichiometries: 1:0.5. 1:1 and 1:2. While it was possible to detect a difference in the values of T_1 for the Lorentzian and Gaussian components, they were nearly equal because of spin-spin interactions between the two. In general the spin-lattice relaxation process has its greatest effect when the molecular motion occurs with a correlation time, $\tau_c \sim 0.1/f_o$ where f_o is the spectrometer frequency.[29] Thus, at the minimum, a particular molecular group has a correlation time of 10^{-9} s. The motion responsible for the minima shown in Figure 42 is probably the methylene group motion in the DDH. In previous studies of the DGEBA:DETA system,[16] an observed minimum in T_1 at 288 K was assigned to methyl group rotation in the DGEBA with a correlation time of 10^{-9} s. While the present data do not extend down to 288 K, there is no sign of an approach to a minimum near 288 K. This result is in agreement with our previous hypothesis that the methyl group rotation in the DGEBA produced the minimum, because the MY720 resin lacks these methyl groups and, hence, lacks a minimum T_1 at 288 K.

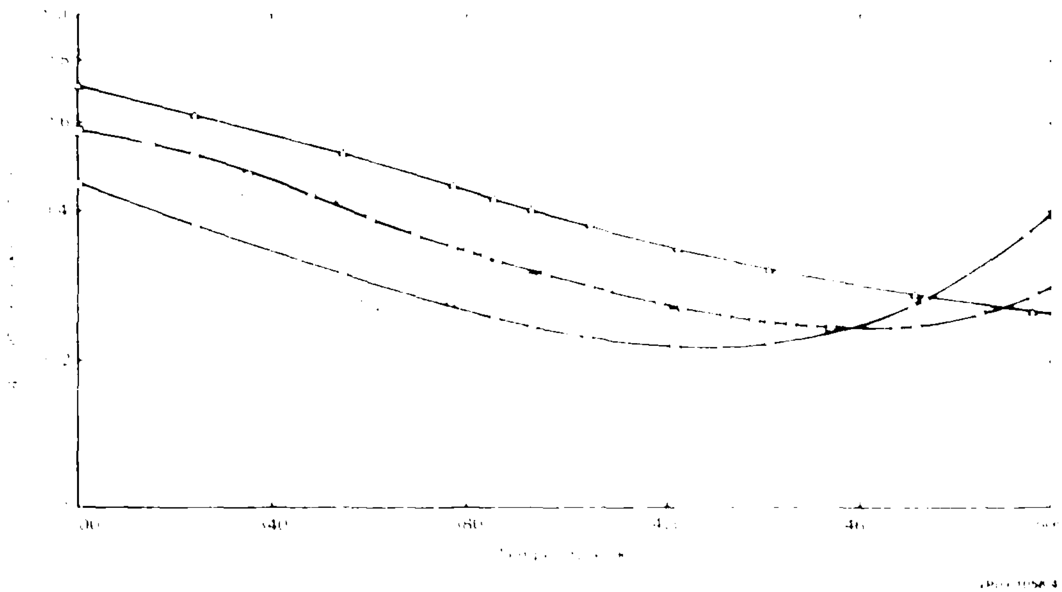

Figure 42. Temperature dependence of the spin-lattice relaxation times for MY720 DDH samples having different stoichiometries.

The assigment of the minimum in T_1 to the methylene group motion is based on two facts. First, the DGEBA:DETA system previously studied also had a high-temperature T_1 behavior, suggesting a minimum above 400 K that was assigned to methylene group motion in the DETA.[16] Second, the rate of spin-lattice relaxation T_1^{-1} increases with increasing DDH content in a manner anticipated, i.e., in a tightly coupled system of spins (hydrogen nuclei) where spin diffusion causes the spins to relax with a common relaxation time T_1,

$$T_1^{-1} = \sum_n F_n T_{1n}^{-1}, \tag{11}$$

where F_n is the fraction of spins, n, whose spin-lattice relaxation time is T_{1n}.[30] If one group of spins dominates the spin-lattice relaxation process, then Equation (11) becomes

$$T_1 = T_{1d}/F_d, \tag{12}$$

where F_d is the fraction of spins dominating the relaxation and T_{1d} is the spin-lattice relaxation time for the process. To determine if the methylene group hydrogens are dominating the relaxation, Equation (12) is written as

$$T_{1CH_2} = T_1 F_{CH_2} . \tag{13}$$

Since T_{1CH_2} at constant temperature is expected to be constant with changing composition, the product of the measured quantities T_1 and F_{CH_2} should be constant if the methylene hydrogens are dominating the spin-lattice relaxation. Results at 380 K, shown in Table 1, are consistent with the methylene hydrogens in the DDH dominating the spin-lattice relaxation, because the product of F_{CH_2} and T_1 is constant to within 4%.

TABLE 1. SPIN-LATTICE RELAXATION AT 380 K.

Stoichiometry MY720 DDH	Calculated fraction of methylene hydrogens F_{CH_2}	Measured T_1 (s)	$F_{CH_2} T_1$ (s)
[illegible]	[illegible]	0.440	0.0783
[illegible]	0.241	0.332	0.0800
[illegible]	0.294	0.252	0.0741

GP03-1058-60

The temperature of the T_1 minimum decreases with increasing DDH content. Thus the correlation time for DDH methylene group motion decreases with an increase in DDH content. If the DDH methylene group motion were independent of DDH content, the temperature of the T_1 minimum would remain constant with increasing DDH, but the value of T_1 at the minimum would decrease. However, these results were not observed. Therefore, the shift in the T_1 minimum to lower temperatures with increasing DDH must be caused by a greater number of unreacted or singly-reacted DDH in the samples with excess DDH. The unreacted and singly-reacted DDH are expected to have greater freedom of motion thus a shorter correlation time.

The rapid motion in the DDH for samples with an excess of DDH can be seen in the hydrogen NMR spectra obtained by Fourier transforming the free-induction decay signals, as shown in Figure 43. The top spectrum is that of a neat MY720 resin. The spectrum was taken at 370 K to reduce the line broadening. The broad low-field line on the left is caused by the aromatic hydrogens, and the broad high-field line is caused by the methylene and

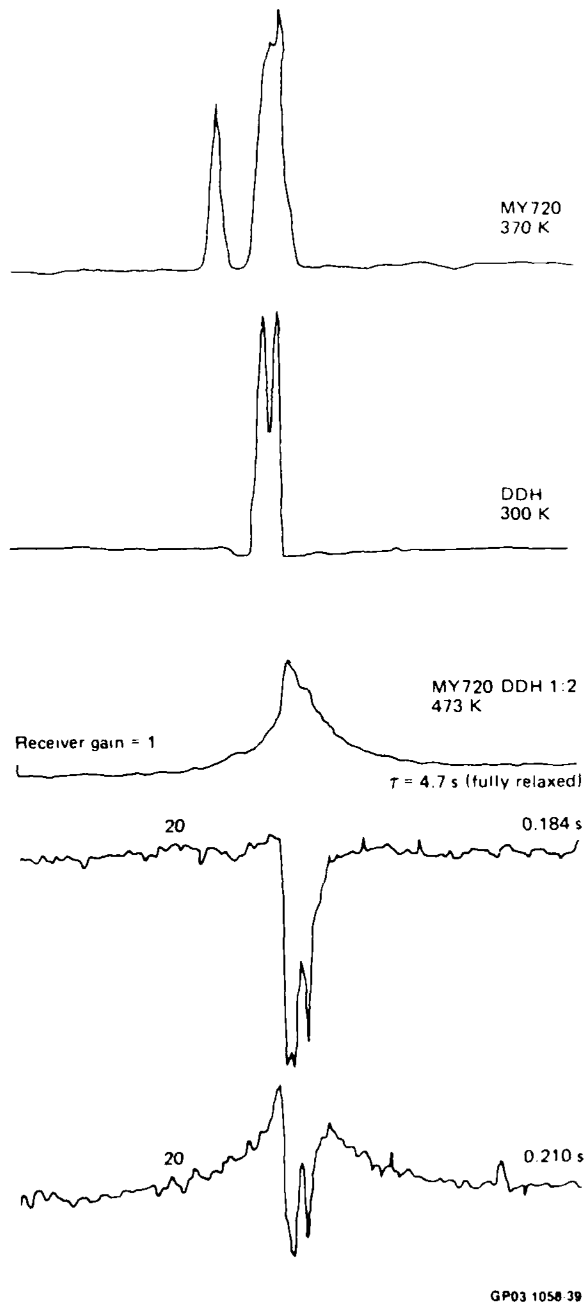

Figure 43. Hydrogen NMR spectra of MY720, DDH, and partially spin-lattice relaxed spectra of 1:2 sample.

methine hydrogens. The spectrum below the MY720 spectrum is that of neat, liquid DDH. The two narrow lines are caused by the methylene and methyl hydrogens. The next three spectra are partially spin-lattice relaxed spectra of an MY720:DDH, 1:2 resin taken at 473 K, above the T_1 minimum. The partially relaxed spectra were obtained by applying a 180° spin inverting pulse, waiting a time τ, applying a 90° pulse, and Fourier transforming the resulting free-induction decay signal. The chemically shifted lines of the different samples are not in exact alignment because of differences in the bulk susceptibilities of the samples; however, the alignment is sufficient to identify the source of the lines. The two narrow, inverted lines in the partially relaxed specra are caused by DDH. Because these lines are narrow, it can be concluded that the DDH producing these lines is undergoing rapid liquid-like motion. Also, because the lines are inverted, it can be concluded that the hydrogen in the DDH producing these lines has a spin-lattice relaxation time T_1 greater than that of the other hydrogen-containing moieties in the sample. This last conclusion requires further explanation because in the previous paragraphs it was stated that the methylene hydrogen in the DDH had a small T_1 at high temperature and was the dominant source of the spin-lattice relaxation. The explanation given below will attempt to show that the DDH motion has a wide range of correlation times.

The temperature dependence of T_1, shown in Figure 42, will aid this explanation. First it will be recalled that as the temperature increases, the correlation time τ_c for molecular motion decreases, and when τ_c is equal to $0.1/f_0$, T_1 is a minimum. Figure 42 and Table 1 suggest that the DDH motion is responsible for the T_1 minimum because T_1 decreases with increasing DDH content in the expected manner. Also, because the temperature at which the minimum occurs decreases with increasing DDH content, it can be concluded that excess DDH acts to decrease the correlation time for DDH molecular motion. This last result supports the hypothesis that the DDH molecular motion is dependent upon whether the DDH is doubly reacted, singly reacted, or not reacted and can explain the partially spin-lattice relaxed spectra. At 473 K (above the T_1 minimum for the 1:2 sample), not all the DDH has the same motional correlation time. The DDH producing the two narrow, inverted lines has a motion with $\tau_c << 10^{-9}$ s. This rapid motion both narrows the linewidth and increases the spin-lattice relaxation time. Similarly the DDH contributing to the broad, upright line has a motion with $\tau_c \sim 10^{-9}$ s so that it is effective in causing the spin-lattice relaxation as stated in the previous paragraphs.

3.5 Temperature-Dependent NMR Measurements of Wet Samples

Temperature-dependent NMR measurements were performed on MY720:DDH samples having a 1:1 stoichiometry and containing ≈ 10 wt% sorbed H_2O. Because the samples lost sorbed water, the high temperature data may lack the precision obtained with the dry samples. The spin-spin relaxation data, Lorentzian fraction data, and spin-lattice relaxation data for both wet and dry samples are shown in Figures 44, 45, and 46 respectively. The T_{2G} and F_L data show a reduction in the glass transition temperature for the sample containing sorbed water. Using the temperature at which F_L is equal to 0.5 as an indication of the glass transition temperature, the 10% sorbed water lowers the glass transition by 27 K.

Below, the glass transition the Lorentzian fraction F_L is 0.13 ± 0.02. The calculated fraction of hydrogen contained in the sorbed water is less than this, viz., 0.10; hence some of the polymer has been plasticized. The Lorentzian spin-spin relax ion time T_{2L} for this component is approximately 500 μs, larger than the T_{2L} for the dry sample. The Gaussian spin-spin relaxation time T_{2G} at 300 K for the wet samples is 17.0 μs, while it is only 15.5 μs for the dry samples. Thus, the plasticizing effect of the sorbed water was distributed throughout the bulk of the sample. As the temperature was increased, this plasticizing effect became more apparent from the difference between the T_{2G}'s for the dry and wet samples.

The Lorentzian spin-spin relaxation time T_{2L} of the wet samples remained nearly constant as a function of temperature. Futhermore, the values of T_{2G} and T_{2L} did not approach a common limit above the glass transition, as was the case for the dry samples. Instead, above the glass transition, n for the pseudo-Gaussian component decreased from 2 to 1 with increasing temperature to produce a second Lorentzian component (dotted line in Figure 44) whose T_{2L} was less than the T_{2L} of the first Lorentzian component. Thus, while the total signal became entirely Lorentzian, it consisted of two Lorentzian components, indicating that two phases were still present above the glass transition temperature. The two T_{2L}'s are plotted in Figure 44, and the fraction of the

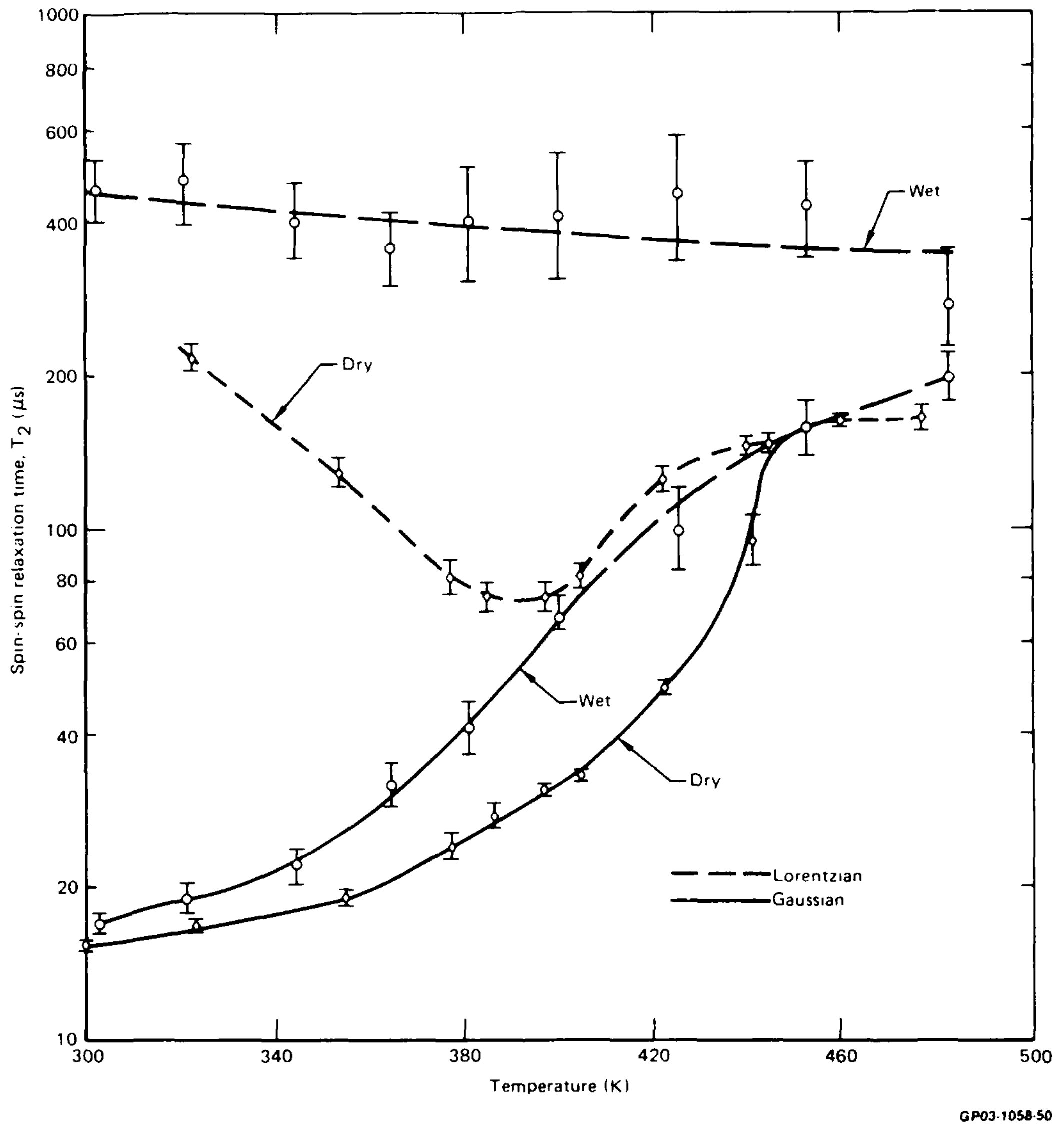

Figure 44. Temperature dependence of the spin-spin relaxation times for dry and wet (10 wt% H_2O) 1:1, MY720:DDH samples.

total signal producing the component with the larger T_{2L} is plotted as a dotted line in Figure 45. The Lorentzian fraction for this component having the larger T_{2L} is seen in Figure 45 to be 0.23 ± 0.03, which is about twice the value of F_L below the glass transition. These data are insufficient to identify the origin of this high-temperature Lorentzian component, but since its spin-spin relaxation time remained nearly constant from below the glass transition to above the glass transition, it is probably associated with the

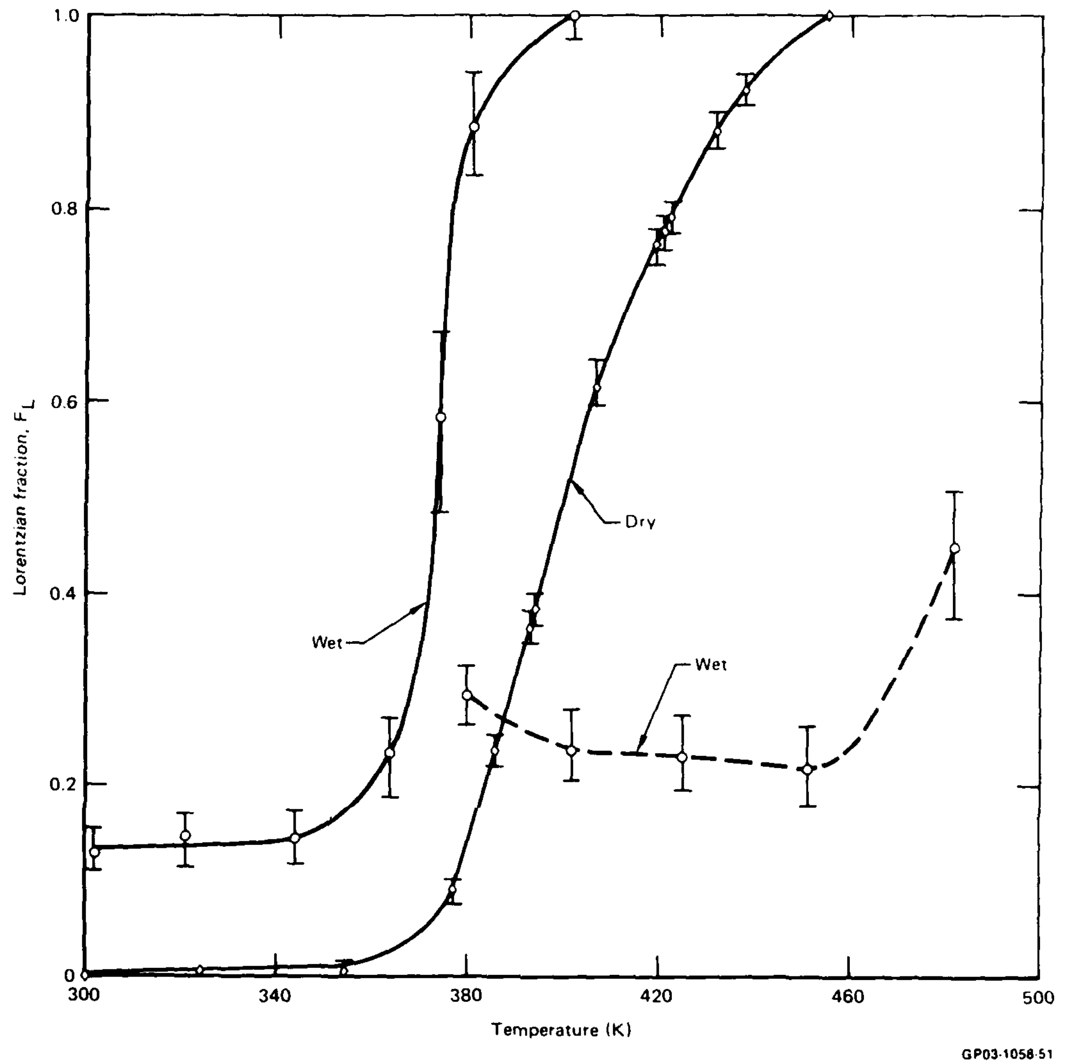

Figure 45. Temperature dependence of the Lorentzian fraction for dry and wet (10 wt% H_2O) 1:1, MY720:DDH samples. The dotted line indicates the fraction of a second Lorentzian component.

sorbed water and the regions of the resin which are strongly plasticized by the sorbed water. Above the glass transition (≈ 460 K), the T_{2L} of the dry samples is about equal to the smaller T_{2L} of the wet samples, so that it appears that similar molecular motion occurred in the dry samples and particular regions of the wet samples, i.e., the nonplasticized regions. This strongly suggests that some regions of the cured epoxy are more readily plasticized than others.

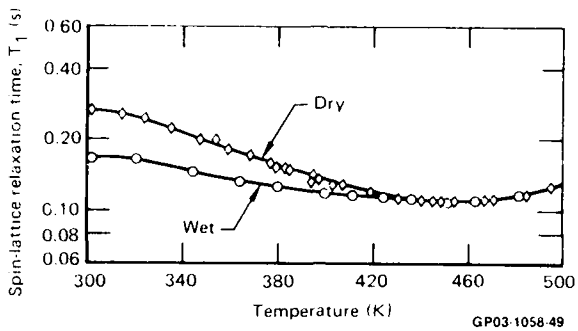

Figure 46. Temperature dependence of the spin-lattice relaxation time for dry and wet (10 wt% H_2O) 1:1, MY720:DDH samples.

The spin-lattice relaxation data shown in Figure 46 are consistent with the foregoing discussion. At lower temperatures the sorbed water probably plasticizes singly-reacted DDH, and the resulting motion 's effective for spin-lattice relaxation. Hence T_1 for the wet samples i significantly less than T_1 for the dry samples. At higher temperatures, the T_1 of both the wet and dry samples were the same. Hence the high-temperature thermally induced motions in the rigid regions of the wet and dry samples must be similar. This same conclusion was deduced in the preceeding paragraph from the T_{2L} data and suggests the presence of two regions in the cured epoxy regins, one easily plasticized (mobile region) and one not easily plasticized (rigid region).

3.6 Determination of the Sizes of the Mobile and Rigid Regions

The presence of both Lorentzian (mobile) and Gaussian (rigid) components in the free-induction decay signals of both wet and dry epoxy resins suggests that spatially separated phases exist within epoxy resins. However, it is possible that a two-component free-induction decay can result from a wide distribution of correlation times for molecular motion.[31] Also, cross correlation effects in molecules moving anisotropically can cause a non-exponential free-induction decay.[32] Resing[31] suggested the use of the Goldman-Shen[28] experiment to help resolve the cause of the two components in a free-induction decay. The Goldman-Shen experiment has previously been used to confirm phase separation in polyurethanes.[15]

The Goldman-Shen pulse sequence is shown in Figure 47; below the pulse sequence are shown the Lorentzian and Gaussian spin systems (hydrogen nuclei) and the NMR signals that result from the pulses. Prior to the first pulse, the spins are aligned along the z-axis, the direction of the laboratory field. Following the first 90° pulse, the conventional free-induction decay signal, consisting of a rapidly relaxing Gaussian signal and a slowly relaxing Lorentzian signal, results. At a time shortly after the Gaussian signal decays to zero but before the Lorentzian signal decays signficantly ($\approx$ 50 μs), a -90° pulse is applied. This -90° pulse returns nearly all of the spins contributing to the Lorentzian signal back along the z-axis, as they were before the first pulse. The spins contributing to the Gaussian signal are randomly oriented and have no net magnetization along the z-axis. During the time τ, spin-spin coupling occurs between the spins contributing to the Lorentzian signal and the spins contributing to the Gaussian signal. This coupling results in a loss of z-magnetization of the spins contributing to the Lorentzian signal and a gain of z-magnetization of the spins contributing to the Gaussian signal, as shown at 5 ms. This exchange of z-magnetization is shown schematically in Figure 47 by three Lorentzian spins losing their alignment with the z-axis and three Gaussian

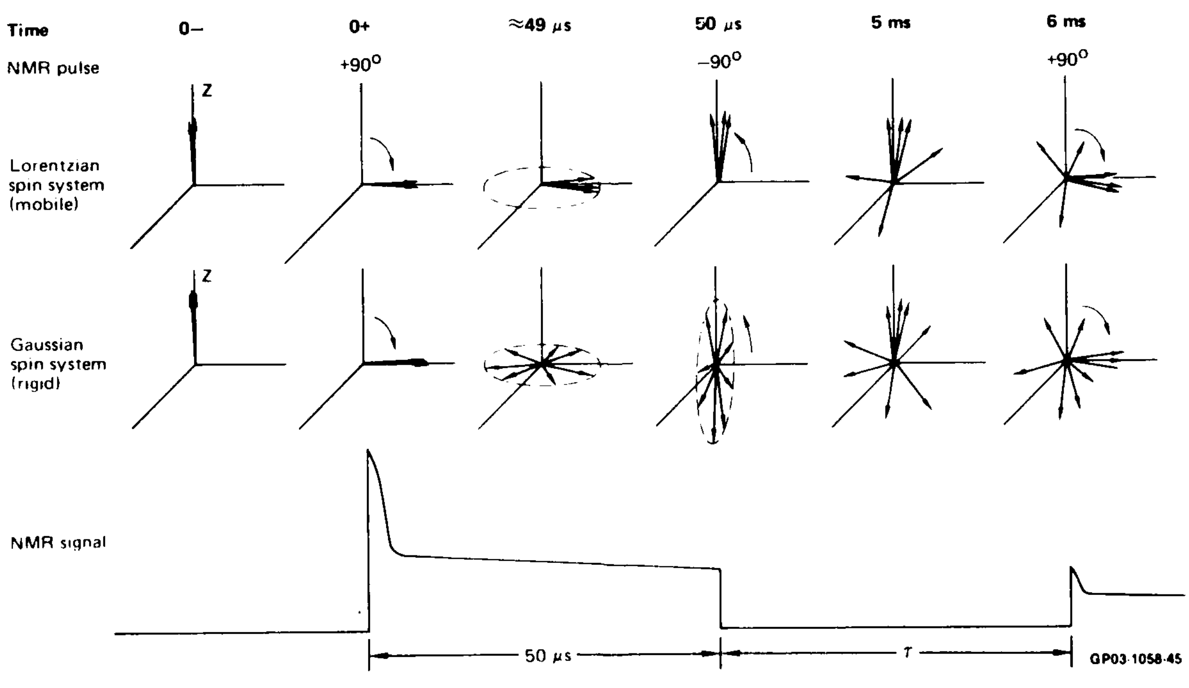

Figure 47. Goldman-Shen pulse sequence.

spins becoming aligned along the z-axis. If the Lorentzian and Gaussian signals have their origin in spatially separated regions, the exchange of z-magnetization occurs by a series of mutual spin flips between nearest neighbors. This exchange is a diffusion phenomenon whose progress can be monitored at various times τ by applying another 90^{o} pulse, as shown at 6 ms, to examine the relative amplitudes of the Lorentzian and Gaussian signals. As shown in Figure 47, after 6 ms, the Gaussian signal increases at the expense of the Lorentzian signal. The rate at which this exchange takes place is used to determine the size of the mobile regions.

The preceding description of the Goldman-Shen experiment for determining the size of the mobile region is expanded in Figures 48 and 49 using fluid[33] and electrical[34] analogies. The z-component of nuclear magnetism is

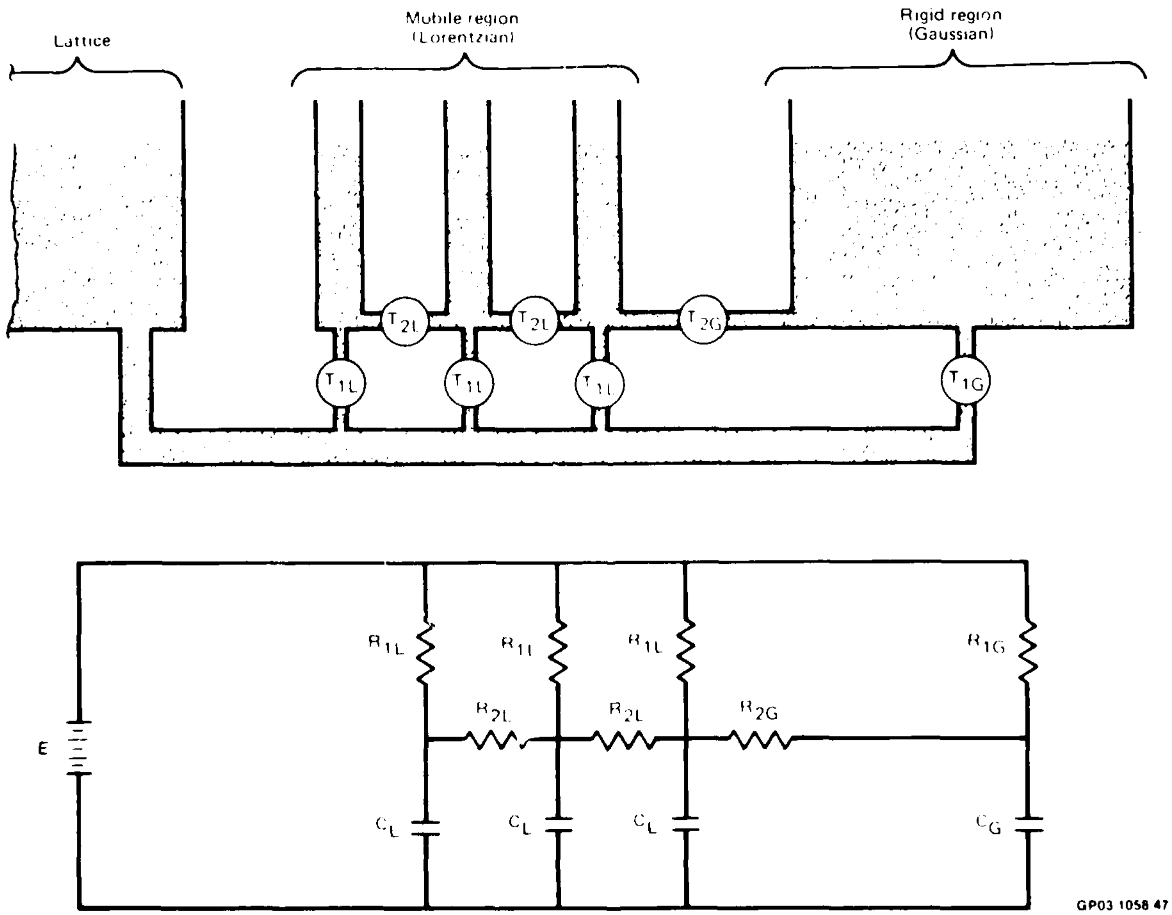

Figure 48. Fluid and electrical models for the NMR relaxation behavior of two-phase polymers.

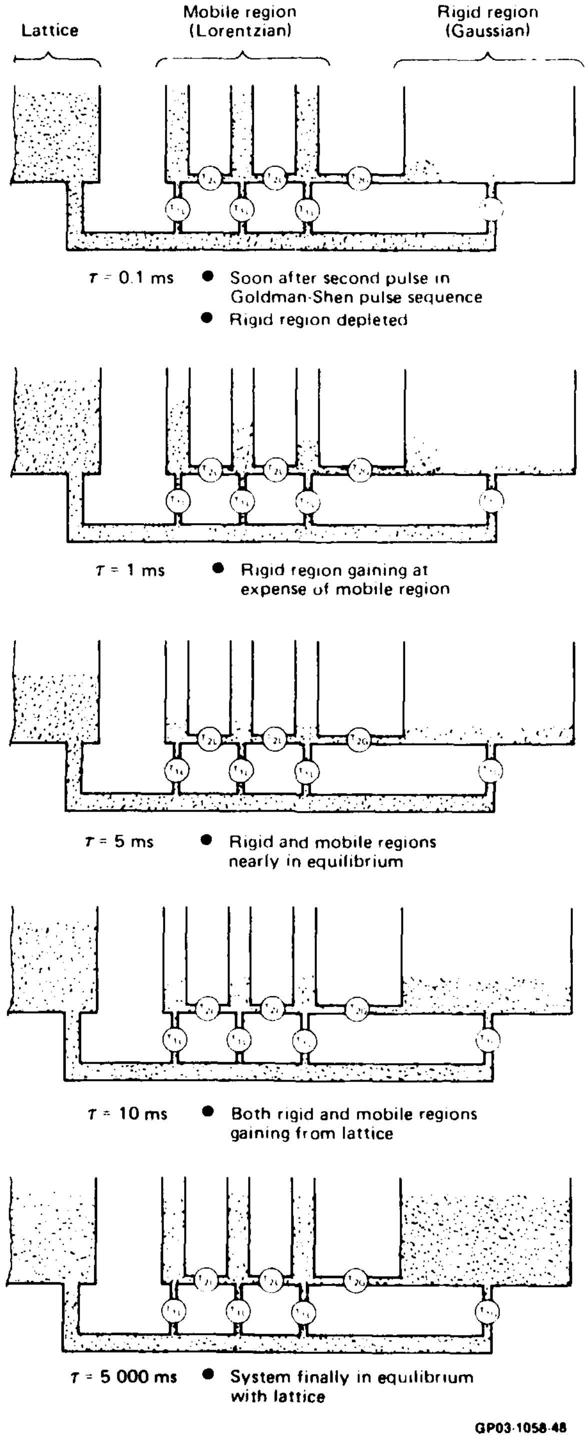

Figure 49. Fluid model of the Goldman-Shen relaxation.

represented by the amount of the fluid in the reservoirs (charge Q on the capacitors). Therefore, the total amount of fluid in the mobile region is proportional to the amplitude of the Lorentzian signal, and the amount of fluid in the rigid region is proportional to the amplitude of the Gaussian signal. The size of the reservoir (capacity C of capacitor) is proportional to the number of nuclear spins in that part of the region. The spin-spin interactions which couple the nuclei together are represented by the T_2 valves (R_2 resistors). Because the Gaussian spin-spin relaxation time T_{2G} is so short compared to the Lorentzian spin-spin relaxation time T_{2L}, the T_2 valves (R_2 resistors) are omitted in the rigid region. The number of reservoirs (capacitors) in the mobile region is proportional to the size of the mobile region. The spin-lattice interactions that couple the nuclei to the lattice are represented by the T_1 valves (R_1 resistors). Because the lattice is a much larger system, the level of the fluid in the lattice reservoir (voltage on the battery) does not change.

Figure 49 illustrates the relaxation process that occurs in the Goldman-Shen experiment following the first two pulses which null the z-magnetization in the Gaussian region. The top illustration at τ = 0.1 ms shows that the fluid level is nearly zero in the rigid region, but fluid is pouring in rapidly (in a time of the order of $T_{2L} \approx 300$ μs) from the adjacent mobile region and trickling in slowly (in a time of the order of $T_{1G} \approx 0.5$ s) from the lattice. At τ = 1 ms the mobile region reservoir adjacent to the rigid region is nearly empty, but the more distant mobile region reservoirs are still nearly full. Thus the fluid in the entire mobile region does not pour into the rigid region in a short time of the order of T_{2L}, but pours in over a longer period dependent upon the physical size of the mobile region. The length of the period determines the size of the mobile region. At 5 ms the relaxation between the mobile and rigid regions is almost complete, as shown by the nearly equal fluid levels in the mobile and rigid regions. At later times, or possibly during the approach to equilibrium between the mobile and rigid regions, the spin-lattice relaxation causes the reservoirs to fill from the lattice reservoir. If the spin-lattice relaxation occurs too rapidly, it can mask the relaxation between the mobile and rigid regions, and an accurate determination of size of the mobile region becomes difficult.

Figure 50 presents the calculated charges on the capacitors in an electrical network which simulates the nuclear spin systems in a two-phase polymer. Actual data that will be presented later can be compared with these simulated results. The component values are chosen so that the Lorentzian

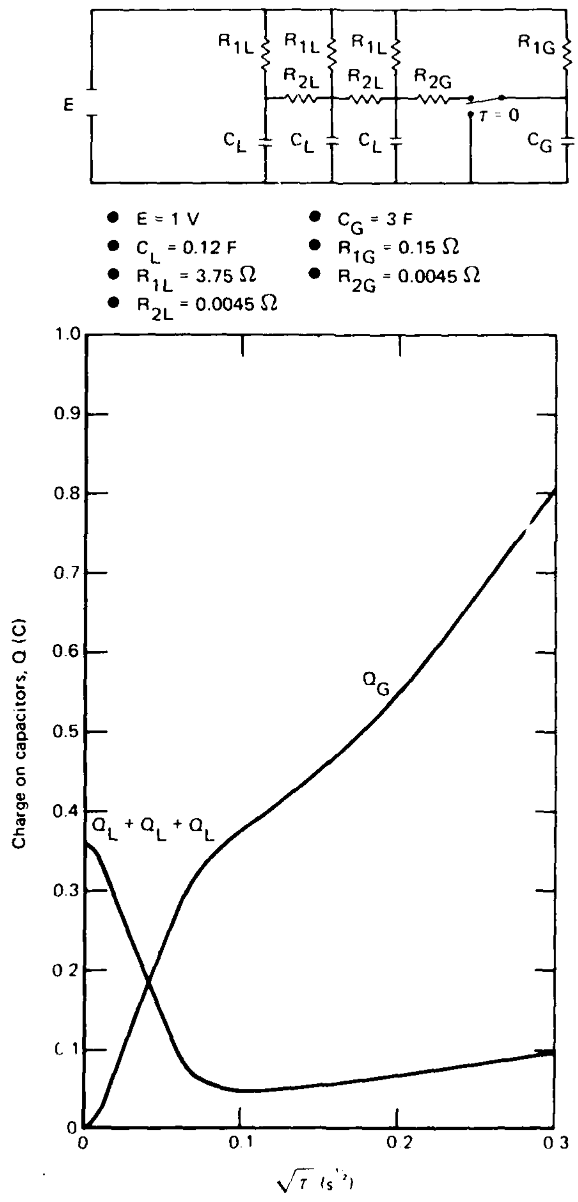

Figure 50. Calculated relaxation of charges on the capacitors in the above circuit after flipping the switch at τ = 0 to the position shown.

fraction F_L (= $3C_L/(3C_L + C_G)$) is 0.107, the spin-lattice relaxation times T_{1L} and T_{1G} (= $R_{1L}C_L$ and $R_{1G}C_G$) are 0.45 s, and the Lorentzian spin-spin relaxation time T_{2L} (= $R_{2L}C_L/2$) is 270 μs. The switch is flipped from the lower position, where the Gaussian capacitor was discharged, to the upper position at $\tau = 0$ to allow the charge Q from the Lorentzian capacitors to leak onto the Gaussian capacitor. The graph below the circuit shows the charges on the capacitors plotted as a function of $\sqrt{\tau}$. Up to about $\sqrt{\tau} = 0.075\ s^{1/2}$, the sum of the charges on the Lorentzian capacitors decreases linearly with $\sqrt{\tau}$, and the charge on the Gaussian capacitor increases linearly with $\sqrt{\tau}$. During this time, little charge is transferred from the lattice, and the sum of the charges on the Lorentzian capacitors plus the charge on the Gaussian capacitor remains nearly constant. Beyond about $\sqrt{\tau} = 0.75\ s^{1/2}$, spin-lattice relaxation effects dominate, and the charges on the capacitors are no longer a measure of the coupling between the Lorentzian and Gaussian regions.

Goldman-Shen experiments were performed on MY720:DDH samples with stoichiometries of 1:0.5, 1:1, and 1:2 that contained sorbed H_2O, D_2O, $CHCl_3$, or $CDCl_3$. Typical free-induction decay signals at various times τ after the first two pulses in the Goldman-Shen pulse sequence are shown in Figure 51. At $\tau = 0.1$ ms the free-induction decay signal is almost totally Lorentzian. At later times the Gaussian signal grows at the expense of the Lorentzian signal. The amplitudes of the Gaussian and Lorentzian signals as a function of $\sqrt{\tau}$ for a 1:0.5 sample containing 7.5 wt% sorbed water are shown in Figure 52. These results are similar to those shown for the electrical analog in Figure 50. In the absence of any other competing relaxation mechanisms, the ratio A_G/A_L in the Goldman-Shen relaxation would approach f_G, the value of A_G/A_L as measured in the simple free-induction decay signal. Also, if the sum of the Gaussian and Lorentzian amplitudes is constant during the Goldman-Shen relaxation, $A_G(\tau) + A_L(\tau) = A_L(0)$, one can calculate the value of A_L needed to yield $A_G/A_L = f_G$: $A_L = A_L(0)/(f_G + 1)$. This value for A_L is indicated in Figure 52 as a horizontal line labeled "Calculated equilibrium A_L." The time required for the diffusion of magnetization from the region containing the Lorentzian component to the region containing the Gaussian component is then determined by the intersection of the extension of the initial straight-line portion of the $A_L(\tau)$ data with the "Calculated equilibrium A_L" line.

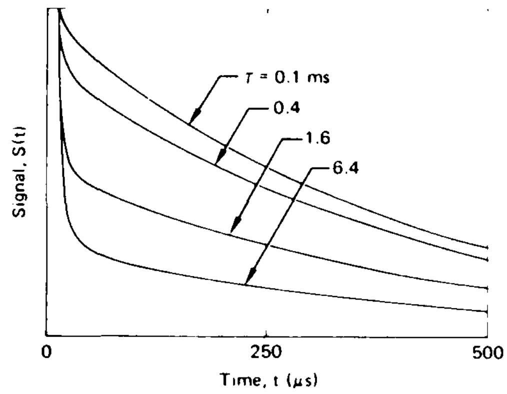

Figure 51. Free-induction decay signals obtained at different times τ in the Goldman-Shen recovery.

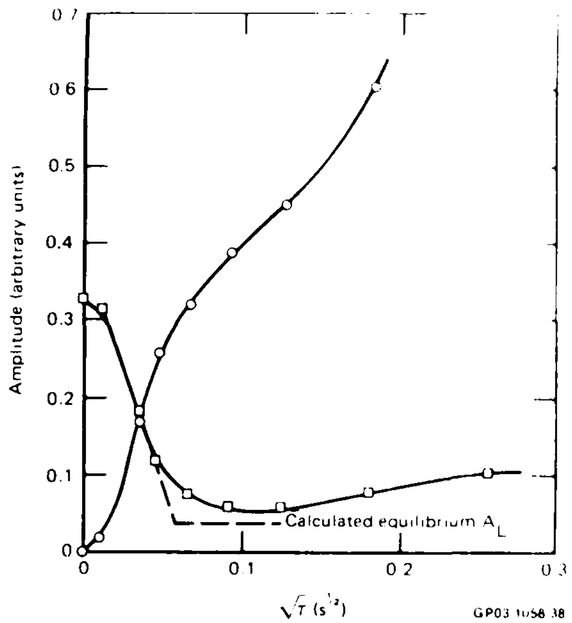

Figure 52. Goldman-Shen relaxation for MY720:DDH, 1:0.5 cured epoxy sample containing 7.5 wt% sorbed H_2O. The Lorentzian amplitude is denoted by (□) and the Gaussian amplitude is denoted by (○).

This diffusion time was used to determine the size of the mobile region. The distance d over which diffusion takes place in a time τ is given to a good approximation by[35]

$$d = \sqrt{\alpha D \tau}, \tag{14}$$

where D is the spin diffusion constant and $\alpha \approx 1$ for a slab geometry, in which case d is the half-thickness of the slab; $\alpha \approx 2$ for a cylindrical geometry, in which case d is the radius of the cylinder; and $\alpha \approx 3$ for a spherical geometry, in which case d is the radius of the sphere. The spin diffusion constant D in a mobile polymer with a spin-spin relaxation time T_{2L} is given by[15]

$$D = \frac{2r_o^2}{T_{2L}}, \tag{15}$$

where r_o is one half the distance between the nearest hydrogens in the polymer, assumed to be 0.125 nm.

The Goldman-Shen relaxation for samples of other stoichiometries containing sorbed H_2O and D_2O are shown in Figures 53 through 57. The measured and derived results for these measurements are shown in Table 2, along with results for samples containing $CHCl_3$ and $CDCl_3$ and a sample at elevated temperature. While small differences in the sizes of the mobile regions exist, the differences are surprisingly small. The results for samples containing sorbed H_2O are similar to those for samples containing sorbed D_2O except for the anomalous results for the 1:1 sample containing sorbed D_2O. These results were at first unexpected because it was thought that the large diffusion constant of H_2O in epoxies $\sim 10^{-12}$ m^2 s^{-1}, which is about 10^4 times larger than the diffusion constant for spin diffusion, would dominate the diffusion process. That is, the H_2O moving rapidly from place to place in the epoxy would transport z-magnetization faster than the slower mutual spin flips between adjacent hydrogens. Because the deuterium in D_2O does not undergo mutual spin flips with the hydrogen in the epoxy, the D_2O would not be able to transport hydrogen z-magnetization by bulk diffusion

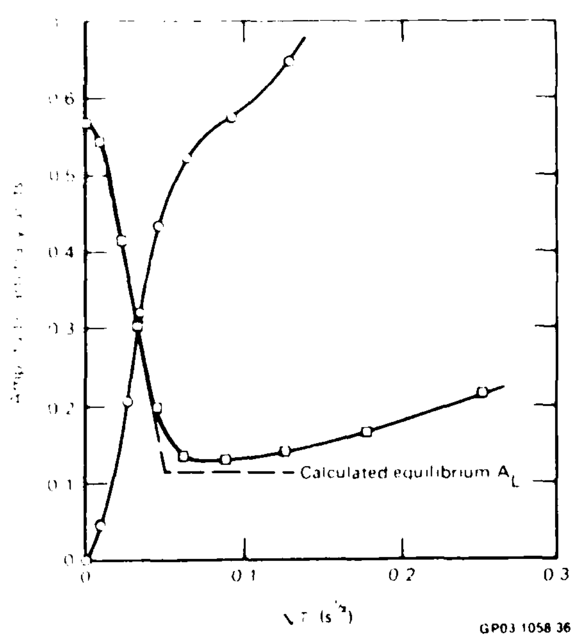

Figure 53. Goldman-Shen relaxation for MY720:DDH, 1:1 cured epoxy sample containing 8.5 wt% sorbed H_2O. The Lorentzian amplitude is denoted by (□) and the Gaussian amplitude is denoted by (○).

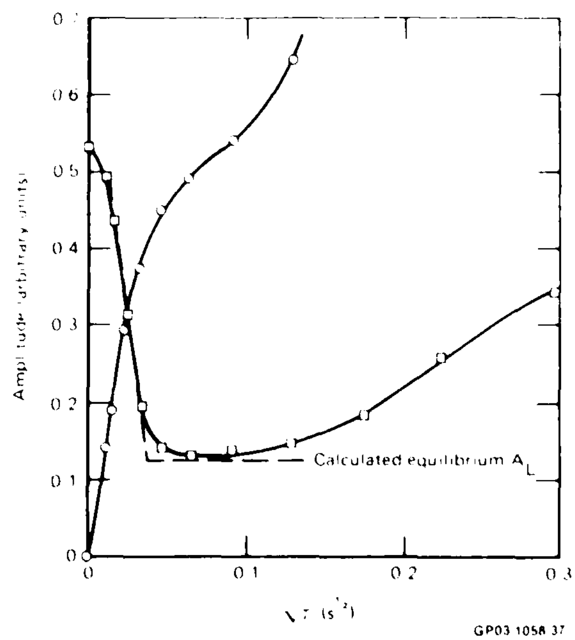

Figure 54. Goldman-Shen relaxation for MY720:DDH, 1:2 cured epoxy sample containing 3.2 wt% sorbed H_2O. The Lorentzian amplitude is denoted by (□) and the Gaussian amplitude is denoted by (○).

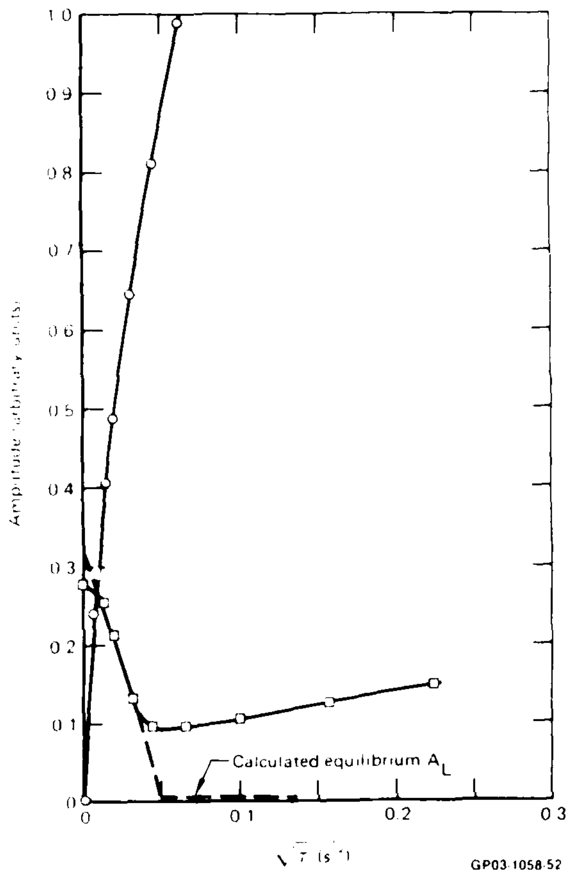

Figure 55. Goldman-Shen relaxation for MY720:DDH, 1:0.5 cured epoxy sample containing 7.3 wt% sorbed D_2O. The Lorentzian amplitude is denoted by (□) and the Gaussian amplitude is denoted by (○).

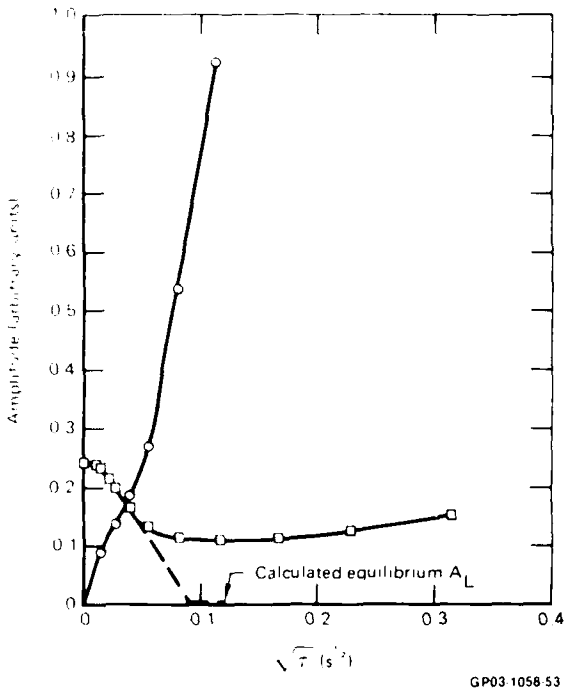

Figure 56. Goldman-Shen relaxation for MY720:DDH, 1:1 cured epoxy sample containing 6.1 wt% sorbed D_2O. The Lorentzian amplitude is denoted by (□) and the Gaussian amplitude is denoted by (○).

TABLE 2. GOLDMAN-SHEN RESULTS FOR MY720:DDH CURED EPOXY.

Sample stoichiometry	Temperature (K)	Sorbed solvent (wt%)	T_2 (μs)	$D \times 10^{16}$ ($m^2 s^{-1}$)	$\sqrt{\tau}$ ($s^{1/2}$)	Half-thickness of mobile region, assuming slab geometry, d (nm)
1:0.5	303	7.5 H_2O	300	1.0	0.058	0.58
1:0.5	303	7.3 D_2O	330	0.95	0.065	0.63
1:1	303	8.5 H_2O	440	0.71	0.051	0.43
1:1	303	6.1 D_2O	370	0.85	0.090	0.83
1:1	303	~30 $CHCl_3$	360	0.87	0.12 ± 0.06*	1.1 ± 0.6*
1:1	303	~30 $CDCl_3$	260	1.2	0.16 ± 0.06*	1.8 ± 0.7*
1:1	383	0	140	2.2	0.037	0.55
1:2	303	8.9 H_2O**	440	0.71	0.036	0.30
1:2	303	8.9 D_2O**	460	0.68	0.046	0.38

GP03 1058 56

*See text for explanation of large errors

**3.2 wt% weight gain, but 5.7 wt% unreacted material was leached from samples

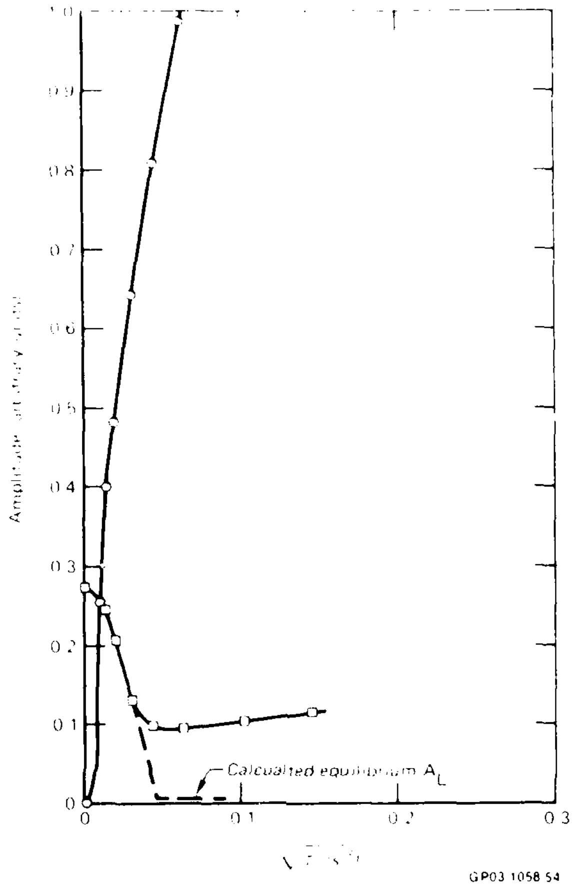

Figure 57. Goldman-Shen relaxation for MY720:DDH, 1:2 cured epoxy sample containing 3.2 wt% sorbed D_2O. The Lorentzian amplitude is denoted by (□) and the Gaussian amplitude is denoted by (○)

through the sample as would the H_2O. Thus the results for deuterated solvents were expected to differ from the results for normal hydrogen containing solvents. (The D_2O contained little HOD as a result of deuterium-hydrogen exchange with labile hydrogen in the epoxy because the HOD was eliminated by performing several changes of D_2O in which the samples were immersed.) However, theoretical studies performed under IRAD funding have shown that these results are correct and the calculated sizes are valid.

The results of the Goldman-Shen experiments yield the size of the mobile regions which can then be used to determine the size of the rigid regions if certain assumptions are made concerning the geometry of the regions. Because the precision of the results do not justify a detailed model of the geometry, a simple geometry is assumed. It is assumed that the rigid, highly crosslinked domains are cubes with sides of length a. It is further assumed that the mobile, low crosslink density regions join the cubes together, like mortar holds bricks together. The total thickness of the mobile regions is 2d, as given in Table 2. Thus, the fraction F_M of the total volume that is mobile is

$$F_M = 1 - \frac{1}{\left(1 + \frac{2d}{a}\right)^3} . \tag{16}$$

Since d is known from the Goldman-Shen results and F_M can be estimated from the Lorentzian fraction, Equation 16 can be solved for a:

$$a = \frac{2d}{(1 - F_M)^{-1/3} - 1} . \tag{17}$$

Table 3 lists the calculated sizes of the rigid regions assuming that F_M is equal to the fractional weight gain F_W of water and also assuming that F_M is equal the Lorentzian fraction F_L. Except for the 1:1 sample containing sorbed D_2O, which seems to be anamolous, the results based on F_W are nearly identical for samples containing sorbed H_2O and D_2O. The size of the rigid regions is about 46 nm for the 1:0.5 sample and decreases to about 22 nm for the 1:2 sample. These results should be compared with electron microscopy results which show that the size of the nodules in the DGEGA:DETA system decreases from 45 nm to 15 nm as the DETA is increased from below stoichiometry to the stoichiometric amount.[5]

TABLE 3. CALCULATED SIZES OF CUBE-SHAPED RIGID REGIONS.

Sample stoichiometry/solvent	Assumed value for volume fraction of mobile region, F_M: Fractional weight gain of solvent, F_W	Assumed value for volume fraction of mobile region, F_M: Lorentzian fraction, F_L	Half-thickness of mobile region, d (nm)	Calculated size of cube, a (nm): Based on F_W	Calculated size of cube, a (nm): Based on F_L
1:0.5/H_2O	0.075	0.096	0.58	44	34
1:0.5/D_2O	0.073	0.0208	0.63	49	179
1:1/H_2O	0.085	0.182	0.43	29	12
1:1/D_2O	0.061	0.0093	0.83	78	533
1:2/H_2O	0.089	0.181	0.30	19	9
1:2/D_2O	0.089	0.0192	0.38	24	117

GP03 1058 61

The calculated sizes of the rigid regions of samples containing sorbed H_2O differ by about a factor of two depending on whether F_W or F_L was used to estimate F_M. These results appear to be acceptable, especially when it is realized that the assumptions made imply the equality of volume, mass, and hydrogen content; these assumptions could easily introduce an ± 30% error.

The calculated sizes of the rigid regions of the samples containing sorbed D_2O that are based on F_L are much larger than the three other calculated sizes. The cause for this discrepancy is the assumed value for the volume fraction of the mobile region, F_M which is much smaller than the other three assumed values. This shows that the volume of the mobile region is larger than the volume that is based on the fraction of the polymer which assumes a Lorentzian character as a result of sorbed water. Thus the water must selectively swell the low-crosslink regions, and the volume of the water in these regions is significantly larger than the volume of polymer that becomes highly mobile as a result water sorption. Under these conditions, the NMR signal from singly reacted (dangling) molecules in regions containing the sorbed water would be Lorentzian. But doubly reacted molecules (or short chains of molecules) which bridge the gap between the adjacent rigid regions would probably produce a Gaussian signal because of their lower mobility. This crosslinkage is a source of error in determining the volume of the mobile region because within the mobile region there could be bridging groups that should correctly be included in the mobile volume, but which produce a rigid (Gaussian) NMR signal. This error tends to underestimate the size of the mobile regions, which then leads to an overestimate of the calculated size of the rigid regions.

As shown in Table 3, the half-thicknesses of the mobile region ranges from 0.30 to 0.83 nm for the samples containing sorbed H_2O or D_2O assuming a slab-like geometry for the mobile regions. This thickness should be compared to the end-to-end distance of the DDH molecule which ranges from ~0.40 nm to ~1.36 nm depending upon whether it is coiled or stretched. Thus, it is conceivable that the mobile regions measured with the NMR consist of DDH molecules that are chemically bound to rigid regions at only one end. Such molecules could have sufficient motional freedom to produce a Lorentzian signal. Recall that the high-temperature NMR spectra, shown in Figure 43, showed two narrow DDH lines, indicating that DDH and not MY720 (at least not the aromatic groups in the MY720) was undergoing extensive molecular motion.

It is reasonable that DDH and not MY720 is the mobile polymer fraction because MY720 can chemically bind at four different locations to either other MY720 or DDH molecules; however, DDH can chemically bind at only two different locations to MY720 molecules, but not to other DDH.

The results for samples containing sorbed $CHCl_3$ or $CDCl_3$, as shown in Table 3, should be regarded as preliminary because they were obtained early in the contract period when an inferior data collection system was used, and insufficient data was collected to reduce the experimental errors to acceptable limits. The sizes of the mobile regions are somewhat larger than those measured in samples containing sorbed water, but further experiments need to be performed before definite conclusions can be reached.

The size of the mobile regions for the 1:1 sample at 383 K, as shown in Table 3, is about 0.55 nm, which is within the range of length for the DDH molecule. This result at only one temperature should also be regarded as preliminary.

3.7 DGEBA Samples

Preliminary experiments were performed on cured DGEBA samples. The primary purpose of these experiments was to provide information useful for interpreting the results of the MY720:DDH studies. This study did not prove to be the case, and detailed studies were not performed. The results of these experiments are given below.

Stoichiometric mixtures of DGEBA and 1,2-cyclohexanedicarboxylic anhydride (CHCA), containing 1 wt% tripropylamine (TPA), were cured at room temperature and then post-cured at 433 K. Room-temperature NMR measurements were made on these samples before and after immersion in water. The dry samples contained a large Gaussian and small Lorentzian component (F_L = 0.042), but the Lorentzian spin-spin relaxation time T_{2L} was unusually small (~46 μs) indicating little motion. The Gaussian spin-spin relaxation time T_{2G} was 15.3 μs. After immersion in water at 370 K for 200 h, the samples gained only 1.65 wt%. If only this sorbed water contributed to the Lorentzian component, one would predict a Lorentzian fraction F_L of 0.028, while a value of 0.042 was measured. This value was not larger than that measured in the dry sample, but the Lorentzian spin-spin relaxation time T_{2L} increased to 150 μs. The Gaussian spin-spin relaxation time increased slightly to 15.8 μs.

The Goldman-Shen results for this sample yielded a mobile region half-thickness d of 0.75 nm.

DGEBA samples were also cured with stoichiometric amounts of DDH. These samples in their dry state had fairly large Gaussian spin-spin relaxation times T_{2G} (about 20 μs) which indicated a low crosslink density. This result was expected because both DGEBA and DDH are bifunctional and tend to produce linear polymers. Crosslinks could form in this system by pendant hydroxyl groups on the linear chain reacting with oxirane rings. These samples gained about 4.5 wt% after immersion at 370 K in H_2O or D_2O for 200 h. Based on this weight gain, a Lorentzian fraction F_L of 0.052 would have been expected for the sample containing sorbed H_2O, assuming that only the hydrogen in the H_2O was mobile. The measured value was 0.074, which was 0.022 more than expected, and represents the mobile polymer. The measured F_L of the sample containing sorbed D_2O was only 0.005; one might have expected it to be 0.022 based on the results with sorbed H_2O. However, labile hydrogens in this polymer exchange with deuterium and render them invisible to the hydrogen NMR. These labile hydrogens account for 0.043 of the total number of hydrogens in the polymer and could possibly explain the low measured value of F_L for the sample containing sorbed D_2O. The Gaussian spin-spin relaxation time of the samples containing sorbed H_2O or D_2O was ~25 μs, significantly larger than the 20 μs measured in the dry samples. This large increase was unlike that measured in the anhydride-cured samples which experienced a change from 15.3 to only 15.8 μs as a result of plasticization by sorbed water thereby further indicating that these samples have a low crosslink density.

4. SUMMARY OF CONCLUSIONS

4.1 EPR Conclusions

- MY720 can be spin labeled with nitroxide amines to form either an end-label or a spin-labeled quaternary base.
- The spin-labeled quaternary base can undergo a Hofmann elimination reaction to release the spin probe TEMPENE.
- The nitroxides decompose in the uncured MY720 because the resin contains reactive impurities.
- The spectra of the spin probes or spin labels observed in dry cured epoxies at each temperature can be characterized by one value of the motional correlation time.
- The spectra of the spin probe or spin label in plasticized cured epoxies can be characterized by a bimodal distribution of motional correlation times at some solvent contents.
- The motional correlation times for spin probes in the fast phase in dry cured epoxy samples obey the WLF equation.
- The motional correlation times for spin probes (or spin labels) in the fast phase in cured epoxy samples plasticized with either water or methylene chloride obey the Fujita-Doolittle equation.
- The mobile fraction evaluated from the area under the fast phase spectrum in the plasticized samples is approximately linearly dependent on the solvent volume fraction.
- The superposition of EPR spectra indicates the presence of microstructure in the form of regions of different crosslink density and implies that the plasticizing solvent partitions between the low crosslink regions and the high crosslink regions.
- In the case of the spin labels, the nitroxides in the mobile phase are relaxed by local modes of main-chain motion located in regions of low crosslink density.
- In the case of the spin probes, the nitroxides in the fast phase are relaxed by either main-chain segmental motions or local modes that precede the onset of the main chain segmental motions.

4.2 NMR Conclusions

- Excess DDH in cured MY720:DDH produced samples having lightly crosslinked regions in which the onset of extensive molecular motion occurred at lower temperatures and whose molecular motion was more isotropic above the glass transition.
- The Lorentzian fraction as a function of temperature is a sensitive measure of the glass transition.
- The MY720:DDH, 1:0.5 sample had a higher glass transition temperature and smaller mobility above the transition temperature than the 1:1 or 1:2 samples; hence extensive homopolymerization of the MY720 occurred in the 1:0.5 sample.
- The correlation time τ_c for DDH methylene group motion in cured MY720:DDH samples was 10^{-9} s in the 1:0.5 sample above 500 K, in the 1:1 sample at ~465 K, and in the 1:2 sample at ~425 K.
- At 473 K the partially spin-lattice relaxed NMR spectra of a MY720:DDH, 1:2 sample contained narrow lines, indicating that some of the DDH was undergoing liquid-like motion.
- There was a distribution of motional correlation times for DDH in cured MY720:DDH samples containing sorbed water and/or at elevated temperatures.
- Sorbed water lowered the glass transition temperature as measured with NMR.
- Samples of cured MY720:DDH, 1:1 containing sorbed water exhibited a two-phase behavior both below and above the glass transition temperature.
- Some regions of the cured MY720:DDH samples were more readily plasticized than others.
- Below the temperature of the minimum in the spin-lattice relaxation, sorbed water plasticized the DDH, and the resulting DDH motion caused the spin-lattice relaxation time to decrease.
- The half-thicknesses of the assumed slab-shaped mobile regions in the MY720:DDH system containing sorbed water ranged from 0.30 nm for 1:2 samples to 0.63 nm for 1:05 samples; this size is the order of the end-to-end size of DDH.
- The size of the assumed cube-shaped rigid regions in the MY720:DDH system containing sorbed water ranged from ~19 nm for 1:2 samples to ~44 nm for the 1:0.5 samples.

APPENDIX A: The Equivalence of the Effects of Temperature and Solvent-Induced Free Volume Changes

We show in this appendix that if the modified forms of the WLF (Equation (4)) and Fujita-Doolittle (Equation (7)) equations are obeyed, then $\Delta_T/\delta_T = \Delta_S/\delta_S$.

If

$$\ln \frac{\tau}{\tau_R} = \frac{1}{f_T} - \frac{1}{f_o} \quad \text{(modified WLF equation)}, \tag{A1}$$

then

$$\frac{d\tau}{dT} = -\frac{\tau}{f_T^{\,2}} \frac{df_T}{dT} . \tag{A2}$$

But, since $f_T = f_o + \alpha(T - T_o)$ for $T > T_g$, (A3)

$$\frac{df_T}{dT} = \alpha . \tag{A4}$$

Substituting Equation (A4) into Equation (A2), one obtains

$$1/\delta_T = \frac{d\tau}{dT}\frac{1}{\varepsilon} = -\frac{\alpha}{f_T^{\,2}} \frac{\tau_R}{\varepsilon} \exp\left(\frac{1}{f_T} - \frac{1}{f_o}\right) . \tag{A5}$$

A small variation in free volume fraction, λ, arising from a difference in rigidity will change T_C by Δ_T, which is given by Equation (3), i.e.,

$$f_T + \lambda = f_o + \alpha[(T + \lambda/\alpha) - T_o]$$

$$= f_o + \alpha[(T + \Delta_T) - T_o]$$

so that

$$\Delta_T = \frac{\lambda}{\alpha} . \tag{A6}$$

Using Equation (A5) and Equation (A6), one obtains

$$\frac{\Delta_T}{\delta_T} = -\frac{\lambda}{f_T^{\,2}} \frac{\tau_R}{\varepsilon} \exp\left(\frac{1}{f_T} - \frac{1}{f_o}\right) . \tag{A7}$$

In an analogous manner, if

$$\ln \frac{\tau}{\tau_R} = \frac{1}{f_C} - \frac{1}{f_o} \quad \text{(modified Fujita-Doolittle equation),} \tag{A8}$$

$$\frac{d\tau}{dv_l} = -\frac{\tau}{f_C^{\,2}} \frac{df_C}{dv_l} . \tag{A9}$$

But since $f_C = f_o + \beta v_l$, (A10)

$$\frac{df_C}{dv_l} = \beta .$$

Substituting Equation (A10) into Equation (A9), one obtains

$$\frac{1}{\delta_S} = \frac{d\tau}{dv_l} \frac{1}{\varepsilon} = \frac{-\beta}{f_C^{\,2}} \frac{\tau_R}{\varepsilon} \exp\left(\frac{1}{f_C} - \frac{1}{f_o}\right) . \tag{A11}$$

The variation in free volume fraction, λ, arising from a difference in rigidity will change v_C by Λ_S, which is given by Equation (A10). Thus,

$$f_c + \lambda = f_o + \beta \left(v_l + \frac{\lambda}{\beta}\right) \tag{A12}$$

$$= f_o + \beta(v_l + \Lambda_S)$$

so that

$$\Lambda_S = \frac{\lambda}{\beta} . \tag{A13}$$

Using Equation (A11) and Equation (A13), one obtains

$$\frac{\Lambda_S}{\delta_S} = -\frac{\lambda}{f_C^{\,2}} \frac{\tau_R}{\varepsilon} \exp\left(\frac{1}{f_C} - \frac{1}{f_o}\right) . \tag{A14}$$

Comparing Equations (A7) and (A14) at the same free volume contents, i.e., where $f_T = f_C$, it can be seen that

$$\frac{\Delta_T}{\delta_T} = \frac{\Lambda_S}{\delta_S} . \tag{A15}$$

In the above, the following notation is used:

δ_T The temperature range where the motional correlation time goes from the slow (10^{-7} s) to the fast regime (10^{-9} s) (see Figure 35).

δ_S The solvent range where the motional correlation time goes from the slow to the fast regime (see Figure 35).

T_C The critical temperature which characterizes the onset of the motional narrowing.

Δ_T The half-width of the distribution of T_C values.

v_C The critical solvent volume fraction which characterizes the onset of the motional narrowing.

Δ_S The half-width of the distribution of v_C values.

f_T The free-volume fraction at temperature T.

f_o The free-volume fraction at a reference temperature and zero solvent content.

τ The motional correlation time for the spin probe.

τ_R The motional correlation time at a reference temperature and solvent content.

α The thermal expansion coefficient.

ε The difference in motional correlation times for the slow and fast regimes.

λ Change in free-volume fraction.

f_C The free-volume fraction at a given solvent volume fraction.

v_1 Solvent volume fraction.

β Proportionality constant between v_1 and f_C.

REFERENCES

1. A. S. Kenyon and L. E. Nielson, Characterization of Network Structure of Epoxy Resins by Dynamic Mechanical and Liquid Swelling Tests, J. Macromol. Sci. A3, 275 (1976).
2. R. E. Cuthrell, Macrostructure and Environment Influenced Surface Layer in Epoxy Polymers, J. Appl. Polymer Sci. 11, 949 (1967).
3. J. L. Racich and J. A. Koutsky, Nodular Structure in Epoxy Resins, J. Appl. Polymer Sci. 20, 2111 (1976).
4. J. S. Mijovic and J. A. Koutsky, The Effect of Postcure Time on the Fracture Properties and Nodular Morphology of an Epoxy Resin, J. Appl. Polymer Sci. 23, 1037 (1979).
5. J. Mijovic and J. A. Koutsky, Correlation Between Nodular Morphology and Fracture Properties of Cured Epoxy Resins, Polymer 20, 1095 (1979).
6. R. J. Maty, D. R. Uhlmann, and J. A. Koutsky, Structure of Glassy Polymers, Small Angle X-Ray Scattering from Epoxy Resins, J. Polymer Sci. 18, 1053 (1980).
7. R. J. Morgan and J. E. O'Neal, The Microscopic Failure Processes and Their Relation to Structure of Amine-Cured Bisphenol A Diglycidyl Ether Epoxies, J. Mater. Sci. 12, 1966 (1977).
8. C. E. Browning, The Effects of Moisture on the Properties of High Performance Structural Resins and Composites, Technical Report AFML-TR-72-94 (1972).
9. L. J. Berliner, Ed., Spin Labeling: Theory and Applications (Academic Press, New York, 1976)
10. D. Kivelson, The[illegible]SR Linewidths of Free Radicals, J. Chem. Phys. 33, 1094 (1960)
11. J. H. Freed, Theory of Slow Tumbling ESR Spectra for Nitroxides, Spin Labeling: Theory and Applications (Academic Press, New York, 1976).
12. David W. McCall, Nuclear Magnetic Resonance Studies of Molecular Relaxation Mechanisms in Polymers, Acc. Chem. Res. 4, 223 (1971).
13. A. C. Lind and D. P. Ames, Multiple-Pulse Reduction of Proton Dipolar Broadening in Solid Copolymers, J. Polymer Sci. B12, 339 (1974).
14. V. J. McBrierty, D. C. Douglass, and P. J. Barham, Oriented Polymers from Solution III. NMR of Polyethylene/Polypropylene Blends, J. Polym. Sci., Polym. Phys. Ed. 18, 1561 (1980).

15. R. A. Assink. Nuclear Spin Diffusion Betweem Polyurethane Microphases, Macromolecules 11, 1233 (1978).

16. I. M. Brown, A. C. Lind, and T. C. Sandreczki, Magnetic Resonance Studies of Epoxy Resins and Polyurethanes, Technical Report MDC Q0673. (3 May 1979) Final Report, Naval Air Systems Command Contract N00019-78-C-0031.

17. L. F. Fieser and M. Fieser, Advanced Organic Chemistry, (Reinhold Publishing Corporation, New York, 1961).

18. J. D. Ferry, Viscoelastic Properties of Polymers, (John Wiley, New York, 1980).

19. A. K. Doolittle and D. B. Doolittle, Studies in Newtonian Flow, J. Appl. Phys. 28, 901 (1957).

20. H. Fujita and A. Kishimoto, Interpretation of Viscosity Data for Concentrated Polymer Solutions, J. Chem. Phys. 34, 393 (1961).

21. M. H. Cohen and D. Turnbull, Molecular Transport in Liquids and Glasses, J. Chem. Phys. 31, 1164 (1959).

22. I. M. Brown and A. C. Lind, Study of the Glass Transition in Crosslinked Polymers Using Nuclear and Electron Magnetic Resonance, Technical Report MDC Q0633, Final Report, Naval Air Systems Command Contract N00019-76-C-0565.

23. I. M. Brown, Nitroxide Spin Probe Studies in a Block Copolymer, Macromolecules (accepted for publication).

24. W. G. Miller, University of Minnesota (private communication).

25. Z. Veksli and W. G. Miller, The Effects of Good Solvents on Molecular Motion of Nitroxide Free Radicals in Covalently Labeled Polystyrene and Poly(Methyl Methacrylate), Macromolecules 10, 686 (1977).

26. Z. Veksli and W. G. Miller, The Effect of Solvents on Molecular Motion of Nitroxide Free Radicals Doped in Polystyrene and Poly(Methyl Methacrylate), Macromolecules 10, 1245 (1977).

27. A. C. Lind, A Programmable Digital Pulser for NMR, Rev. Sci. Inst. 43, 1800 (1972).

28. M. Goldman and L. Shen, Spin-Spin Relaxation in LaF_3, Phys. Rev. 144, 321 (1966).

29. N. Bloembergen, E. M. Purcell, and R. V. Pound, Relaxation Effects in Nuclear Magnetic Resonance Absorption, Phys. Rev. 73, 679 (1948).

30. J. E. Anderson and W. P. Slichter, Nuclear Spin Relaxation in Solid n-Alkanes, J. Phys. Chem. 69, 3099 (1965).

31. H. A. Resing, Distribution of Motional Correlation Times: NMR Spectroscopy, Adv. Mol. Relaxation Processes 3, 199 (1972).

32. P. S. Hubbard, Nonexponential Relaxation of Three-Spin Systems in Nonspherical Molecules, J. Chem. Phys. 51, 1647 (1969).

33. A. N. Garroway, W. G. Moniz, and H. A. Resing, Carbon-13 NMR in Organic Solids: The Potential for Polymer Characterization, Am. Chem. Soc. Symposium Series 103, 67 (1979).

34. A. Kalk and H. J. C. Berendsen, Proton Magnetic Relaxation and Spin Diffusion in Proteins, J. Mag. Res. 24, 343 (1976).

35. R. B. Bird, W. E. Stewart, and E. N. Lightfoot, Transport Phenomena 356-358 (John Wiley and Sons, Inc., New York, 1960).

DISTRIBUTION

	Copies
Commander, Naval Air Systems Command Department of the Navy Attn: Code AIR-5163D5 Washington, DC 20361	8
Commander, Naval Air Systems Command Department of the Navy Attn: Code AIR-320A Washington, DC 20361	1
Commander, Naval Air Systems Command Department of the Navy Attn: Code AIR-954 (DDC) Washington, DC 20361	12
Director, Naval Research Laboratory Washington, DC 20375 Attn: Code 6110	1
Code 6120	1
Code 6170	1
Commander, Naval Surface Weapons Center Attn: Code WR-31 White Oak Silver Spring, MD 20910	2
Commanding Officer Naval Ship R&D Center Annapolis Laboratory Annapolis, MD 21402	1
Commander, Naval Air Development Center Attn: Code 606 Warminster, PA 18974	2
Commander, Naval Weapons Center Attn: Code 385 China Lake, CA 93555	1
Office of Naval Research Attn: Code 472 800 N. Quincy St. Arlington, VA 22217	1

	Copies
Office of Naval Research Boston Branch Office Attn: L. H. Peebles 495 Summer St. Boston, MA 02210	1
Army Materials & Mechanics Research Center Attn: Dr. George Thomas Watertown, MA 02172	2
U. S. Army Research Office Attn: Dr. John Hurt Box CM, Duke Station Durham, NC 27706	1
Director, Air Force Materials Laboratory Wright Patterson AFB, OH 45433 Attn: Code AFWAL/MLBE	1
Code AFWAL/MLXE	1
Code AFWAL/MLBC	1
Code AFWAL/MLBP	1
Air Force Office of Scientific Research Attn: D. R. Ulrich Bolling Air Force Base Washington, DC 20332	1
NASA Headquarters Materials & Project Office Attn: Mr. Charles F. Bersch 600 Independence Ave., S.W. Washington, DC 20546	1
NASA Langley Research Center Attn: Dr. N. Johnston Head, Polymer Group Hampton, VA 23665	1
NASA Lewis Research Center Attn: R. W. Lauver Cleveland, OH 44135	1
National Bureau of Standards Institute for Materials Research Attn: Dr. Leslie Smith Washington, DC 20234	1

Copies			Copies
Plastics Technical Evaluation Center Picatinny Arsenal Attn: Code DRDARSCM-O Dover, NJ 07801	1	Grumman Aerospace Corporation Attn: Mr. H. Borstell Bethpage, LI., NY 11714	1
Acurex/Aerotherm Attn: Mr. Robert Washburn 485 Clyde Avenue Mountain View, CA 94042	1	Hercules, Inc. Attn: Dr. R. E. Hoffman P. O. Box 98 Magna, UT 84044	1
Fred A. Keimel, President Adhesive & Sealants Newsletter P. O. Box 72 Berkeley Heights, NJ 07922	1	ITT Research Institute 10 W. 35th Street Chicago, IL 60616	1
Aerospace Corporation Attn: W. J. Versino P. O. Box 92957 Los Angeles, CA 90009	1	University of California Lawrence Livermore Laboratory Attn: T. T. Chiao P. O. Box 808 Livermore, CA 94550	1
Battelle Columbus Laboratories 505 King Avenue Columbus, OH 43201	1	Lockheed California Company Dept. 74-54, Bldg 63 Attn: Mr. J. H. Wooley Box 551 Burbank, CA 91503	1
The Boeing Company Aerospace Group Attn: Mr. Clyde H. Sheppert P. O. Box 3999 Seattle, WA 98124	1	Lockheed Missile & Space Co., Inc. Attn: Clayton A. May P. O. Box 504 Sunnyvale, CA 94088	1
CIBA-GEIGY Corporation Plastics & Additives Division Attn: Raymond Seltzer Ardsley, NY 10502	1	University of Maryland Attn: Dr. W. J. Bailey College Park, MD 20742	1
General Dynamics Corporation Convair Division Attn: Mr. Ed Harrison San Diego, CA 92138	1	Polymer Research Institute University of Massachusetts Amherst, MA 01002	1
General Electric R&D Center P. O. Box 8 Schenectady, NY 12301	1	McDonnell Douglas Corporation Attn: Dr. James Carpenter P. O. Box 516 St. Louis, MO 63166	1
Goodyear Aerospace Corporation Attn: Hugh Boyd Akron, OH 44315	1	New York University Dept. of Applied Science Attn: Dr. Walter Brenner Barney Building 26-36 Stuyvesant St. New York, NY 10003	1

	Copies
Northrop Corporation Attn: D. Crabtree (Nonmetallic Research Dept.) 3901 W. Broadway Hawthorne, CA 90250	1
Northwestern University Dept. of Materials Science & Engineering Attn: Dr. J. O. Brittain Evanston, IL 60201	1
Columbus Aircraft Division Rockwell International Attn: J. Fasold 4300 E. Fifth Avenue Columbus, OH 43216	1
Southwest Research Institute Attn: W. E. Woolam 1150 Connecticut Ave., Suite 613 Washington, DC 20036	1
Stanford Research Institute 333 Ravenswood Avenue Menlo Park, CA 94025	1
University of Tennessee Polymer Science & Engineering Program Attn: Prof. John F. Fellers 419 Dougherty Engineering Bldg. Knoxville, TN 37916	1
TRW Attn: R. W. Vaughn One Space Park Redondo Beach, CA 90278	1
United Technologies Research Center Attn: Dr. Dan Scola East Hartford, CT 06108	1
Vought Corporation Advanced Technology Center P. O. Box 6144 Dallas, TX 75222	1

	Copies
Vought Corporation Aeronautics Division Attn: A. Hohman P. O. Box 5907 Dallas, TX 75222	1
Westinghouse Corporation R&D Center Attn: Z. N. Sanjana 1310 Beulah Road Pittsburgh, PA 15235	1

DATE
ILMED
-8